

# We are IntechOpen, the world's leading publisher of Open Access books Built by scientists, for scientists

6,900

Open access books available

186,000

International authors and editors

200M

Downloads

Our authors are among the

154

Countries delivered to

TOP 1%

most cited scientists

12.2%

Contributors from top 500 universities



WEB OF SCIENCE™

Selection of our books indexed in the Book Citation Index  
in Web of Science™ Core Collection (BKCI)

Interested in publishing with us?  
Contact [book.department@intechopen.com](mailto:book.department@intechopen.com)

Numbers displayed above are based on latest data collected.  
For more information visit [www.intechopen.com](http://www.intechopen.com)



# Fabrication of Large Core Yb<sub>2</sub>O<sub>3</sub> Doped Phase Separated Yttria-Alumino Silicate Nano-Particles Based Optical Fiber for Use as Fiber Laser

M. C. Paul<sup>1</sup>, A. V. Kir'yanov<sup>2</sup>, S. Bysakh<sup>3</sup>, S. Das<sup>1</sup>, M. Pal<sup>1</sup>, S. K. Bhadra<sup>1</sup>, M. S. Yoo<sup>4</sup>, A. J. Boyland<sup>4</sup> and J. K. Sahu<sup>4</sup>

<sup>1</sup>Fiber Optics and Photonics Division, Central Glass & Ceramic Research Institute (CGCRI), CSIR, Jadaupur,

<sup>2</sup>Centro de Investigaciones en Optica, Guanajuato,

<sup>3</sup>SEM-ESCA Laboratory, Central Glass & Ceramic Research Institute (CGCRI), CSIR, Jadaupur,

<sup>4</sup>Optoelectronics Research Center (ORC), University of Southampton, Southampton,

<sup>1,3</sup>India

<sup>2</sup>Mexico

<sup>4</sup>UK

## 1. Introduction

Development of new rare-earth (RE)-doped optical fibers for high power amplifiers and lasers require continuous improvements in the fiber spectroscopic properties like gain and efficiency characteristics, resistance to spectral hole burning and photodarkening (PD) phenomena besides reduction in device size and economical efficiency. Silica glass as a host material for fibers has proved to be very attractive though some potential applications of RE-doped fibers suffer from limitations in terms of spectroscopic properties resulting from clustering or inappropriate local environment when doped into silica. Several mixed-oxide and non-oxide alternatives to silica have been successfully proposed to obtain spectroscopically improved amplifying single mode fibers in spite of fabrication difficulties and high cost.

The route of interest here consists of using silica as a mechanical host and support of the fiber optical waveguide, and of embedding RE-ions within oxide nanoparticles of composition and structure different from those of silica. When nanoparticles have a crystalline structure the glass becomes transparent glass ceramics (Gonçalves et al., 2002). However, the nanoparticle may also be amorphous, such as those obtained by phase separation (Zarzycki, 1991). Some reports on RE-doped transparent glass ceramic based single mode fibers use low melting mixed oxides prepared by a rod-in-tube technique (Samson et al., 2002), or mixed oxyfluorides using a double-crucible technique (Samson et al., 2001). However, the low melting point of these materials causes low compatibility with

silica components. Transition metal-doped silica-based transparent ceramic fibers were prepared by MCVD (modified chemical vapor deposition) process and using a slurry method (Yoo et al., 2003), where the particles were synthesized before insertion into the silica tube substrate.

Over the past several decades considerable work have been carried out on incorporation of RE oxide nano-crystallites into different glass hosts. Different processes have been developed such as the co-sputtering technique (Fujii et al., 1998), pyrolysis (John et al., 1999), ion implantation (Chryssou et al., 1999), laser ablation (Nichols et al., 2001) and sol-gel processes (Yeatman et al., 2000). Another process which has recently been developed by a Finnish company, Liekki, is the direct deposition of nano-particles (Rajala et al., 2003). In addition, Leikki Company (Koponen et al., 2006) proposed an amplification fiber doped with RE element nano-particles. Compared to conventional Er doped active fiber; it has many advantages in optical gain, amplification bandwidth, photo-darkening, efficiency, quenching phenomena, etc. All these processes are related to the outside vapour deposition technique except for the sol-gel, which involves longer preform fabrication time. Many applications of nano-fiber have been found in telecommunication and sensor such as chemical sensor (Shi et al., 2007) and fiber ring laser (Jiang et al., 2007). An alternative technology is to dope nano-materials into optical fiber. Cho et al. (Cho et al., 2001) doped PbTe nano-particles into optical fiber core and demonstrated its nonlinear optical features. Dove et al. (Dove et al., 2001) fabricated a glass optical fiber doped with Cd<sub>3</sub>P<sub>2</sub> nano-material, obtaining a gain of 7.1dB in a 4 mm-length special fiber. Kawanishi et al. (Kawanishi et al., 2006) injected semiconductor quantum dots solution into a holey optical fiber.

On the other hand solution doping technique (Bandyopadhyay et al., 2004; Bhadra et al., 2003; Sen et al., 2005; Townsend et al., 1987) in the modified chemical vapour deposition (MCVD) method (Li, 1985) is the most common way to incorporate the RE ions into the core of silica optical fiber preform. However, the incorporation of REs into a suitable nano-crystalline host that are dispersed within the silica rich matrix of optical fiber preform, through MCVD and solution doping process is challenging compared to the fabrication of such type of bulk material by normal crucible melting process. In earlier work, we have reported the synthesis of Er<sub>2</sub>O<sub>3</sub> doped phase-separated amorphous nano-particles into calcium-germano silicate core glass host by applying the basic principle of phase-separation phenomena (Blanc et al., 2009). This is to improve the spectroscopic properties of Er-doped fiber, mainly the spectral broadening of fluorescence band.

RE ions into nano-crystalline hosts becomes very important as it experience very dissimilar site and different crystalline fields which give rise to broadening of the individual stark levels. When the RE ions are confined in crystalline environments of low phonon energy, they yield large excited state lifetime and absorption cross-section compared to vitreous surroundings. Generally, Yb<sup>3+</sup> in Y<sub>2</sub>O<sub>3</sub> or YAG (Y<sub>3</sub>Al<sub>5</sub>O<sub>12</sub>) nano-crystalline low silica host exhibits a promising material for high power, high brightness, and high efficiency laser systems because of its small quantum defect between the pump and lasing transitions (Shirakawa et al., 2004). Furthermore, the glass host matrix in which the nano-crystals are immersed possesses the chemical durability and mechanical property of oxide glass. To develop more efficient fiber laser sources based on rare-earths doped materials, hosts with low phonon energies are required. This lower phonon energy reduces significantly non-

radiative decay due to multi-phonon relaxation, allowing increased lifetime of some excited levels that can relax radiatively or can store energy for further up-conversion, cross-relaxation, or energy transfer processes. Considering such importances, the incorporation of Yb<sub>2</sub>O<sub>3</sub> into yttrium-alumino silicate phase-separated nano-crystallites was reported within the core region of silica preform through chemical impregnation of porous phospho-silicate or pure silica layer deposited via MCVD process followed by post-thermal treatment of the preform (Paul et al., 2010).

Yb<sup>3+</sup> in Y<sub>2</sub>O<sub>3</sub> or YAG nano-crystalline host is suitable for making up-conversion and high power lasers (De et al., 2006; Lu et al., 2008a, 2008b; Mun et al., 2005; Patra et al., 2005; Shirakawa et al., 2003; Vetrone et al., 2003). Various Yb<sub>2</sub>O<sub>3</sub> doped host materials have been progressively investigated earlier for fiber lasers, and the Yb:YAG laser is scaled up to an average power of 60 W with an 810-fs duration in a laser with thin-disk geometry (Innerhofer et al., 2003). Yb-doped sesquioxides (RE<sub>2</sub>O<sub>3</sub>, RE = Y, Sc, Lu) serve as potential alternatives to Yb:YAG for power scaling because of their desirable thermal properties. In addition, the strong electron-phonon interaction causes characteristic spectral broadening, especially in the case of Y<sub>2</sub>O<sub>3</sub>. Due to these characteristics, Yb-doped sesquioxides are expected to be a promising laser material for high-power and ultrashort pulse lasers. In this work Y<sub>2</sub>O<sub>3</sub> was selected as an attractive host material for laser applications as it is a refractory oxide with a melting point of 2380°C, a very high thermal conductivity,  $k_{Y_2O_3} = 27$  W/mK, two times YAG's one,  $k_{YAG} = 13$  W/mK. Another interesting property allowing radiative transitions between electronic levels is that the dominant phonon energy is 377cm<sup>-1</sup> which is one of the smallest phonon cutoff among oxides (Ubal dini & Carnasciali, 2008).

Laser operation has been also demonstrated with sesquioxide crystals fabricated by melt-growth methods (Petermann et al., 2002) and a mode-locked Yb<sup>3+</sup>:Sc<sub>2</sub>O<sub>3</sub> crystalline laser has also been reported (Klopp et al., 2003). The laser ceramics based on rare-earth-doped Y<sub>2</sub>O<sub>3</sub>, (Y<sub>0.5</sub>Gd<sub>0.5</sub>)<sub>2</sub>O<sub>3</sub>, Sc<sub>2</sub>O<sub>3</sub>, and Lu<sub>2</sub>O<sub>3</sub> with neodymium (Lu et al., 2001) and ytterbium (Takaichi et al., 2004) have been demonstrated. The passive mode locking of a diode-pumped Yb<sup>3+</sup>:Y<sub>2</sub>O<sub>3</sub> ceramic laser was demonstrated (Shirakawa et al., 2003, 2004). The lasing of the 1 at.% Yb:YAG ceramic laser was also demonstrated with the maximum output power of 1.02 W and a slope efficiency of 25% (Yusong et al., 2007). All such type of glass ceramic based laser containing Y<sub>2</sub>O<sub>3</sub> or YAG crystals possesses low lasing efficiency. Here we have made Yttria alumino rich Yb<sub>2</sub>O<sub>3</sub> doped silica glass based phase-separated nano-particles containing optical fibers to demonstrate good lasing efficiency where the maximum vibrational energy in YAS (Y<sub>2</sub>O<sub>3</sub>-Al<sub>2</sub>O<sub>3</sub>-SiO<sub>2</sub>) glass (Jander and Brocklesby, 2004) is about 950 cm<sup>-1</sup> which is less than the Maximum vibrational energy value of 1100 cm<sup>-1</sup> in silica glass (Tomozawa & Doremus, 1978).

Considering the importance of Yb:YAG nano-crystals as a lasing host, we have reviewed here the formation of such type of nano-crystals within the silica based core glass matrix of optical fiber preform by solution doping technique under suitable thermal annealing conditions. In this paper, we have discussed about the formation of nanostructure in optical fiber samples made from the annealed nano-crystalline host based preform. The role of phosphorous (P) and fluorine (F) was studied on the formation of Yb<sub>2</sub>O<sub>3</sub> doped yttrium-alumino silicate phase-separated crystalline nano-particles. Study of the nature of the particles within the doping host of optical fibers was also done. The change in the local environments of Yb<sup>3+</sup> ion was elucidated from the high-resolution transmission electron microscopy imaging, electron diffraction, X-ray diffraction analyses. The average dopant

levels within the core region were evaluated by electron probe micro-analyses (EPMA). We also report the critical fabrication parameters, the material characterization results, spectroscopic properties, PD phenomena along with their lasing characteristics of such kind of optical fibers.

The purpose of this work is to develop nano-engineering glass based large core optical fibers having diameter around 20-35 micron containing  $\text{Yb}_2\text{O}_3$  doped phase separated nano particles which may improve the photo-darkening phenomenon, lasing property of the fibers mainly the lasing efficiency as well as spectral broadening of the lasing spectrum compared to the normal  $\text{Yb}_2\text{O}_3$  doped YAG crystal based ceramic laser (Yusong et al., 2007) as well as normal alumino-silica based optical fibers.

## 2. Fabrication of nano-engineering glass based optical preforms and fibers

### 2.1 Benefit of the choice of $\text{Yb}_2\text{O}_3$ into nano-crystalline host

- Rare-earth ions into nano-crystalline hosts experience very dissimilar side and experience different crystalline fields, which give rise to broadening of the individual stark levels. When the rare-earth-doping ions are confined in crystalline environments of low phonon energy, it yields large excited state lifetime and optical absorption cross-section compared to vitreous surroundings (Shirakawa et al., 2004).
- Generally  $\text{Yb}^{3+}$  in  $\text{Y}_2\text{O}_3$  or  $\text{Y}_3\text{Al}_5\text{O}_{12}$  nano-crystalline low silica host exhibit a promising material for high power, high brightness, and high efficiency laser systems because of its small quantum defect between pump and lasing transitions (Shirakawa et al., 2004).
- Another interesting property allowing radiative transitions between electronic levels is that the dominant phonon energy is  $377\text{cm}^{-1}$  which is one of the smallest phonon cutoff among oxides (Ubal dini & Carnasciali, 2008).
- Such nano-crystalline structures will be obtained after a thermally controlled growth of the crystal phase directly in the bulk glass through suitable thermal treatment after making of optical preform.
- Purposes of the work is to develop the glass preforms for drawing into Yb-doped optical fibers where nano-structuration of the host should result in improvement of the characteristics of Yb-doped fiber lasers.

### 2.2 Mechanism of the formation of phase-separated nano-engineering glass based optical preform

Incorporation of glass formers and modifiers occurs through solution doping process followed by the MCVD technique. Under appropriate perturbation, such as a thermal treatment, the glass forming the core will be separate into two phases of low and rich silica content, respectively. As the low-silica phase constitutes a small portion of the total core volume, microparticles or even nanoparticles may be expected.

Doping of Yb ion into lithium-aluminosilicate based glass containing  $\text{Y}_2\text{O}_3$  was done through solution doping process followed by phase separation technique in which addition of  $\text{P}_2\text{O}_5$  serve as a nucleating agent to increase phase separation with generation of  $\text{Yb}_2\text{O}_3$  doped micro or nano-crystallites into the core matrix of optical preform. The glass formers incorporated by the vapour phase deposition process involves  $\text{SiO}_2$ ,  $\text{P}_2\text{O}_5$  along with glass modifiers  $\text{Al}_2\text{O}_3$ ,  $\text{BaO}$ ,  $\text{Li}_2\text{O}$ ,  $\text{Yb}_2\text{O}_3$  and  $\text{Y}_2\text{O}_3$  incorporated by solution doping technique.

Incorporation occurs through viscous sintering phenomena. At sintering temperature the core glass will be in a metastable immiscibility under condition of  $T_C$  (crystallization temperature)  $< T_m$  (melting temperature) where phase separation kinetics are faster than crystallization kinetics. More and more negative value of the free energy change of the system for mixing of the oxide components greater will be the phase separation. The core composition of the doping host was modified to minimize the larger phase-separation along with crystallization through optimization of the doping levels of P<sub>2</sub>O<sub>5</sub>, Y<sub>2</sub>O<sub>3</sub> and Al<sub>2</sub>O<sub>3</sub> along with Li<sub>2</sub>O content with incorporation of the other dopants such as BaO so that the following conditions are satisfied:-

- The core glass should be in high transparency to obtain low optical scattering
- Closely matched indices of refraction
- Low birefringency crystals
- Crystal size much smaller than wavelength of light
- Particle size  $< 15$  nm
- Interparticle spacing 15 nm
- Narrow particle size distribution
- No crystal clustering

Liquid-liquid phase separation is a common and well-known phenomenon in silicate liquids, and can be observed in the high-silica regions of many binary and more complex systems, at temperatures either above or below the liquidus (Vogel, 1994). As the field strength (charge/radius) of the modifier oxide cation increases, the resulting consolute (critical) temperatures  $T_c$  become systematically higher (Hageman and Oonk, 1986; Hudon & Baker, 2002). Thermodynamically, it results from strongly positive heats of mixing between SiO<sub>2</sub> and modifier oxide components in silica-rich liquids (Hudon & Baker, 2002), microscopically, the clustering of nonbridging oxygens around high field strength modifier cations lowers energy by facilitating local charge balance and, if extensive enough, stabilizes two coexisting liquids. Here phase-separation has been induced in the clear glasses through suitable thermal annealing process with the appearance of either a crystalline or amorphous phase separation.

One of the reasons may be that yttria-alumino silicate glass undergoes phase-separation under suitable doping levels of Al<sub>2</sub>O<sub>3</sub> and Y<sub>2</sub>O<sub>3</sub> where the glass enters within the immiscible region of yttria-alumino silicate (YAS) glass. A ternary diagram of YAS glass system was shown in Fig. 1 derived from FactSage (Facility for the analysis of chemical thermodynamics) 5.5 thermo chemical software and database. The composition of such kind of glass having silica content around 90 mol% form both two liquid and clear glass zones. The glass transition temperatures for fluorine doped yttria-alumino-silicate glass based optical preform are found to be between 985 and 1115°C which is explained in Section 3.3. The glass transition temperature of oxide glass is related to a combination of several factors such as the density of covalent cross-linking, the number and strength of the coordinate links formed between oxygen and the cation, and the oxygen density of the network (Ray, 1974). With increasing Y content, more coordinate links are formed between oxygen and yttrium, which is opposed by the lower oxygen density of the network from the more open structure needed to accommodate larger yttrium ions and depolymerization in the network with decreasing silica content or increasing Y/Al. Such type of nano-structuration retain within the core glass matrix of optical fiber.

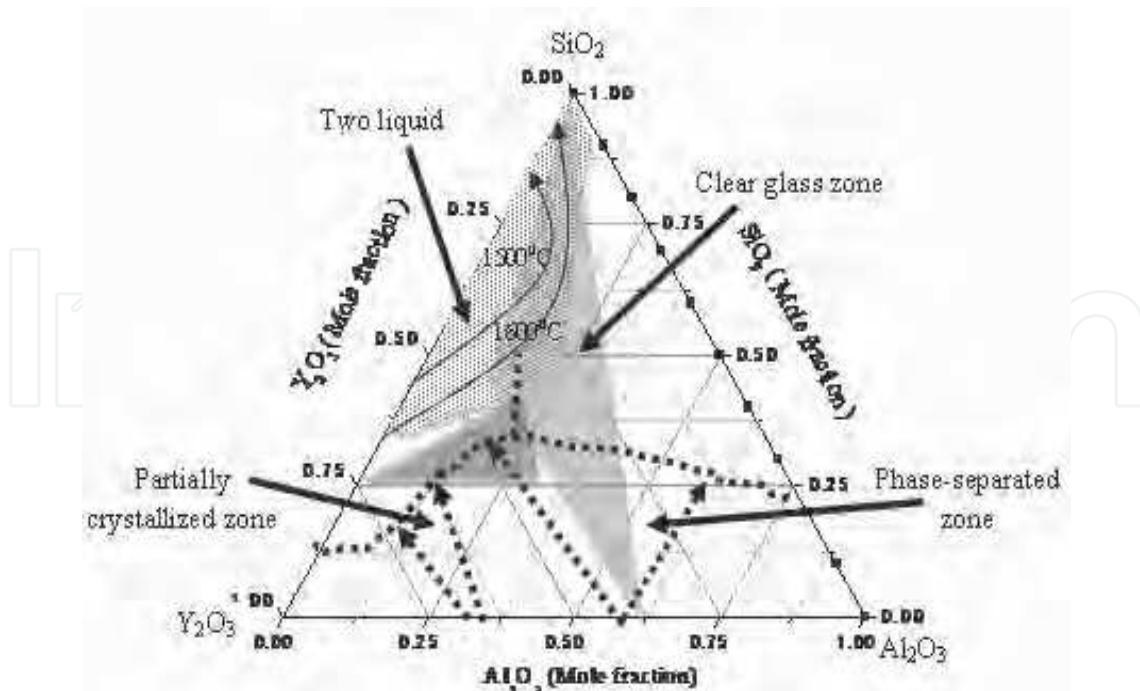


Fig. 1. Phase-diagram of SiO<sub>2</sub>-Al<sub>2</sub>O<sub>3</sub>-Y<sub>2</sub>O<sub>3</sub> system derived from Fact Sage software indicating the partially crystallized, glass forming and phase-separated zones.

### 2.3 Role of different co-dopants for making of nano-engineering glass based optical fibers

- The composition of Yb<sub>2</sub>O<sub>3</sub> doped nano-engineering optical fiber was selected as SiO<sub>2</sub>-P<sub>2</sub>O<sub>5</sub>-Y<sub>2</sub>O<sub>3</sub>-Al<sub>2</sub>O<sub>3</sub>-Li<sub>2</sub>O-BaO.
- P<sub>2</sub>O<sub>5</sub> serve as a nucleating agent for promotion of phase-separation phenomena along with crystallization.
- Y<sub>2</sub>O<sub>3</sub> and Al<sub>2</sub>O<sub>3</sub> serve as a formation of crystalline host of composition of Y<sub>3</sub>Al<sub>5</sub>O<sub>12</sub> under suitable thermal annealing process.
- Li<sub>2</sub>O serve for formation of glass-ceramic based material of composition (lithium alumino-silica) LAS glass to increase the optical transparency of the doping host.
- BaO serve as an agent which increase the glass formation region of the matrix as well as reduce the viscosity of the glass host.
- In some cases fluorine was also incorporated for enhancement of the phase-separation followed by reducing the phonon-energy of the glass host.

### 2.4 Modified chemical vapour deposition (MCVD) process with solution doping technique

Incorporation of Yb ions into nano-engineering glass based on yttria-alumino-silica host was done through solution doping process followed by suitable thermal treatment of the preform (Paul et al, 2010a). The inner diameter of the tube is typically 17.0-18.0 mm. P<sub>2</sub>O<sub>5</sub> was added into the deposited porous layer where P<sub>2</sub>O<sub>5</sub> serve as a nucleating agent to increase the phase separation with generation of Yb<sub>2</sub>O<sub>3</sub> doped micro or nano-crystallites into the core matrix of optical fiber preform. SiO<sub>2</sub> and P<sub>2</sub>O<sub>5</sub> which serve as glass formers were incorporated through the vapour phase deposition process. The glass modifiers such as Al<sub>2</sub>O<sub>3</sub>, BaO, Li<sub>2</sub>O, Yb<sub>2</sub>O<sub>3</sub> and Y<sub>2</sub>O<sub>3</sub> are incorporated by the solution doping technique using

an alcoholic-water (1:5) mixture of appropriate strength of YbCl<sub>3</sub>.6H<sub>2</sub>O, AlCl<sub>3</sub>.6H<sub>2</sub>O, YCl<sub>3</sub>.6H<sub>2</sub>O, LiNO<sub>3</sub> and BaCl<sub>2</sub>.2H<sub>2</sub>O. All the preforms fabricated by the conventional MCVD technique, where the gaseous chlorides vapour of SiCl<sub>4</sub> and POCl<sub>3</sub> including O<sub>2</sub> were passed through a rotating silica tube and heated by an external burner which moves along the tube. Due to high temperature, the chloride precursors oxidise, forming particles which deposit on the inner wall of the tube. At this stage depending upon the radial temperature gradient occurring across the hot zone, a homogeneous gas phase reaction takes place and solid particles nucleate from the reaction products. Particle growth occurs primarily as a result of coagulation of colliding particles as the finely dispersed solids suspended in the gas pass through the radial-gradient of hot zone. Deposition of porous layers occurs through collisions induced by Brownian motion which result in aggregates of individual glass particles. Such kind of deposition is caused by thermophoresis, a phenomenon in which suspended particles experiences a net force in the direction of decreasing temperature due to a greater rate of collisions with gas molecules on the hot side of each particle which sinter together by viscous flow if the glass is sufficiently fluid (Miller & Chynoweth, 1979; Shelby, 1997; Izawa & Sudo, 1987). The deposited porous layer (Fig. 2) after solution doping turned into a glassy layer when the burner passes over it at temperature around 1600°C. In the final stage, the tube was collapsed into a solid preform at a temperature higher than 2000°C. The collapsing phenomenon occurs due to inward viscous flow of mass driven by surface tension and pressure difference between inside and outside of the tube. Controls of flow of O<sub>2</sub>, tube temperature and pressure difference between inside and outside of the tube are very important during collapsing process to maintain circular geometry of core. The diameter of the doped region was increased from 20 to 35 micron through modification of several fabrication parameters such as number of deposited porous layers, composition of deposited porous layers and CSA of the starting deposited tube. The uniform doping levels within the large core fiber preforms was maintained through optimization of the deposition temperature with respect to composition as well as numbers of the deposited porous layers based on enlargement of the silica tube prior to deposition. Large core (1.5-2.85 mm) Yb<sub>2</sub>O<sub>3</sub> doped preforms (Paul et al., 2010b) based on yttria-alumino-silica glass hosts were fabricated through modification of several fabrication parameters such as number of deposited porous layers, composition of deposited porous layers and CSA of the starting deposited tube. To make 19.0-20.0 micron diameter fiber from the preform, we have used 82-85 mm<sup>2</sup> CSA tube having inner diameter of 17.0 mm with deposition of 6 numbers of porous layers at optimum deposition temperature of 1350±10°C. The fiber diameter of 22.0±2.5 μm was drawn from the preform made through deposition of 6 numbers of porous layers at optimum deposition temperature of 1275±10°C using silica tube of CSA of 58-60 mm<sup>2</sup> having inner diameter of 18.0 mm. On the other hand, the fiber diameter of 32±2.5 μm was made from the preform fabricated through deposition of 10 numbers of porous layers at optimum deposition temperature of 1240±10°C within inner surface of silica tube of CSA of 58-60 mm<sup>2</sup> having inner diameter of 22.0 mm enlarged from 18.0 mm inner diameter under suitable pressurization prior to deposition of multiple porous phospho-silica layers. The same composition of deposited porous phospho-silica layer was used at each case. The uniform doping levels within the large core of each fiber preform was maintained through optimization of the deposition temperature with respect to composition and numbers of the deposited porous layers as well as varying the inner diameter of the tube under suitable pressurization prior to deposition. Nano-engineering fibers varying NA between 0.07-0.12 and core diameter ranging from 20 to 35 micron were drawn from the

annealed perform under suitable heating conditions made through modification of several fabrication parameters such as number of deposited porous layers, composition of deposited porous layers and CSA of the starting silica tube with varying the inner diameter of the silica tube under suitable pressurization prior to deposition. The details about the making of large core  $\text{Yb}_2\text{O}_3$  doped nano-engineering glass based optical preform through MCVD process followed by solution doping technique is described below:

The following important parameters are involved in this process.

- Composition of the gas phase mixture within the silica tube
- Number of deposited porous layers with pre-sintering
- Deposition temperature of the porous layers
- Composition of the solution of dopant precursors
- Soaking, drying and heat treatment of solution impregnated porous layers
- Dehydration
- Sintering
- Collapsing process

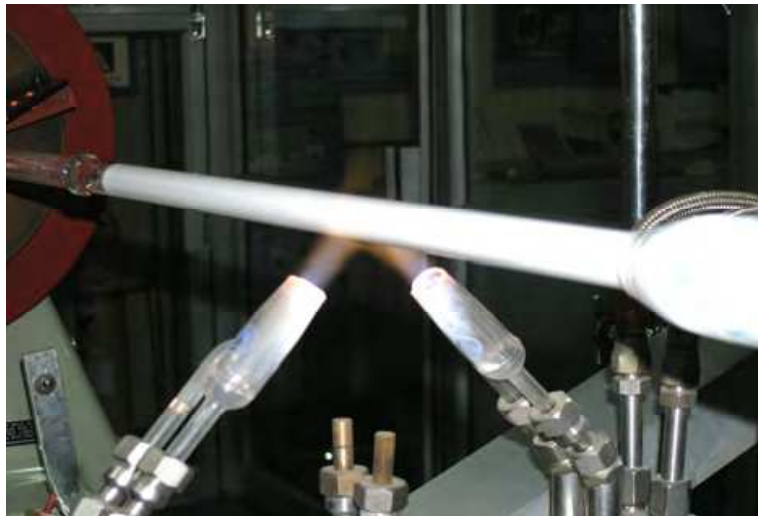


Fig. 2. Deposition of multiple porous layers of composition of  $\text{SiO}_2\text{-P}_2\text{O}_5$  along forward direction by the MCVD process

### 2.5 Composition of the gas phase mixture within the silica tube

The composition of a gas mixture of 13-15 mol% of  $\text{SiCl}_4$ , 1.0-2.0 mol% of  $\text{POCl}_3$ , 2.5-4.0 mol% of He and 79-83.5 mol% of  $\text{O}_2$  was found to be the best for smooth deposition to prevent coagulation of the particles. If coagulation arises, the formation of bubbles starts during sintering stage.

### 2.6 Number of deposited porous layers with pre-sintering

The fiber diameter around 19-20 micron was obtained from the preform made through deposition of maximum 6 numbers of porous silica layers having thickness around  $10\ \mu\text{m}$  containing 0.15 to 0.20 mol% of  $\text{P}_2\text{O}_5$  under optimum deposition temperature of  $1350 \pm 10^\circ\text{C}$  followed by pre-sintering within  $1300\text{-}1350^\circ\text{C}$  which possesses uniform porosity along both axial and radial directions in order to obtain uniform distribution of Al, Yb, Y and Ba ions along the whole diameter (Paul et al., 2010a, 2010b). In this case we have used silica tube of

CSA around  $82\text{-}85\text{ mm}^2$  and inner diameter around  $17.0\text{ mm}$  prior to deposition of porous layers. Under such condition multiple porous layers form uniform networking of the deposited oxide particles between each layer and not disturbed before going to solution impregnation process. From fabrication of a series of large core  $\text{Yb}_2\text{O}_3$  doped nano-engineering preforms shown in Table 1 under different conditions, it was observed that uniform porosity in terms of uniform doping levels of Al, Yb, Y and P ions along the entire core region can be obtained through the way of solution soaking process maintaining uniform thickness ( $10\text{ }\mu\text{m}$ ) of each layer up to deposition of 6 numbers of porous layers under deposition temperature of  $1350\pm 10^\circ\text{C}$  followed by pre-sintering at  $1300\text{-}1350^\circ\text{C}$  (Paul et al., 2010a). The radial view of the microscopic picture (Fig. 3) of such six numbers of multiple porous layers shows a uniform networking of the deposited oxide particles between each layers having uniform thickness of  $10\text{ }\mu\text{m}$  as well as uniform porosity varying slightly within  $\pm 2\%$ .

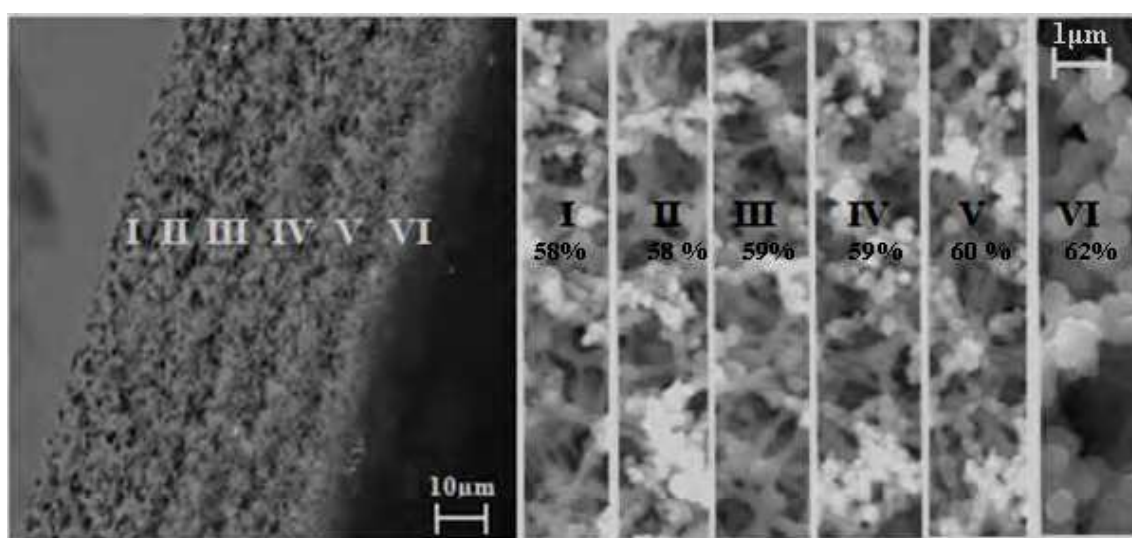


Fig. 3. Radial view of deposited six numbers of phospho-silica layers with the enlarged surface morphology of each layer.

The porosity of the layers varies from 58 to 62% between innermost and outermost layer. The axial view of such thick porous layer shown in Fig. 4 clearly indicates that a uniform networking of the deposited oxide particles between each layer is formed well as observed clearly in the enlarged microscopic view of the particular portion of the deposited layers. The fiber diameter of  $25.0\text{ }\mu\text{m}$  was drawn from the preform made through deposition of 6 numbers of porous layers at optimum deposition temperature of  $1275\pm 10^\circ\text{C}$  using silica tube of CSA of  $58\text{-}60\text{ mm}^2$  having inner diameter around  $18.0\text{ mm}$ . The pre-sintering was done within  $1250\text{-}1275^\circ\text{C}$  for 3 passes. The purpose was to deposit thin ( $8.0\text{-}10.0\text{ }\mu\text{m}$ ) individual layers as shown in Fig. 5a for each deposition pass in order to reduce the penetration length for uniform soaking of the dissolved ions along the radial direction. On the other hand, fiber diameter of  $32\pm 2.5\text{ }\mu\text{m}$  was made from the preform fabricated through deposition of 10 numbers of porous layers at optimum deposition temperature of  $1240\pm 10^\circ\text{C}$  within inner surface of silica tube of CSA of  $58\text{-}60\text{ mm}^2$  having inner diameter around  $22.0\text{ mm}$  enlarged from the initial inner diameter of  $18.0\text{ mm}$  under suitable pressurization. In this case tube was enlarged through suitable pressurization prior to deposition of multiple porous phospho-silica layers. The pre-sintering was done within  $1275$

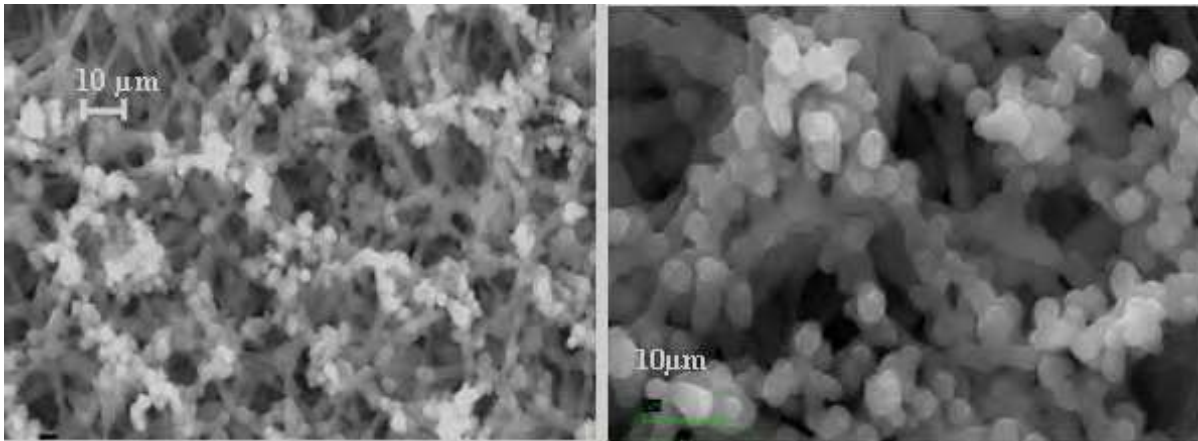


Fig. 4. The microscopic axial view of six multiple porous layers deposited at around  $1350 \pm 10^\circ\text{C}$  along with the enlarged view of the particular portion of the deposited.

to  $1300^\circ\text{C}$  for 3 passes. The radial view of deposited 10 numbers of porous layers having thickness around 5-6 micron was shown in Fig. 5b. To make LMA fibers with core diameter around 30-35 microns, we used thin wall silica tube of cross sectional area (CSA) around 58-60  $\text{mm}^2$  having inner diameter around 18.0 mm of thickness 1.0 mm. The outer surface of such type thin-wall tube was further enlarged to make inner diameter around 22.0 mm under optimum pressurization prior to deposition of multiple porous phospho-silicate layers for getting large core diameter. The purpose was to deposit thin individual layer (5.0-6.0  $\mu\text{m}$ ) for each deposition pass in order to reduce the penetration length for uniform soaking of the dissolved ions along the radial direction.

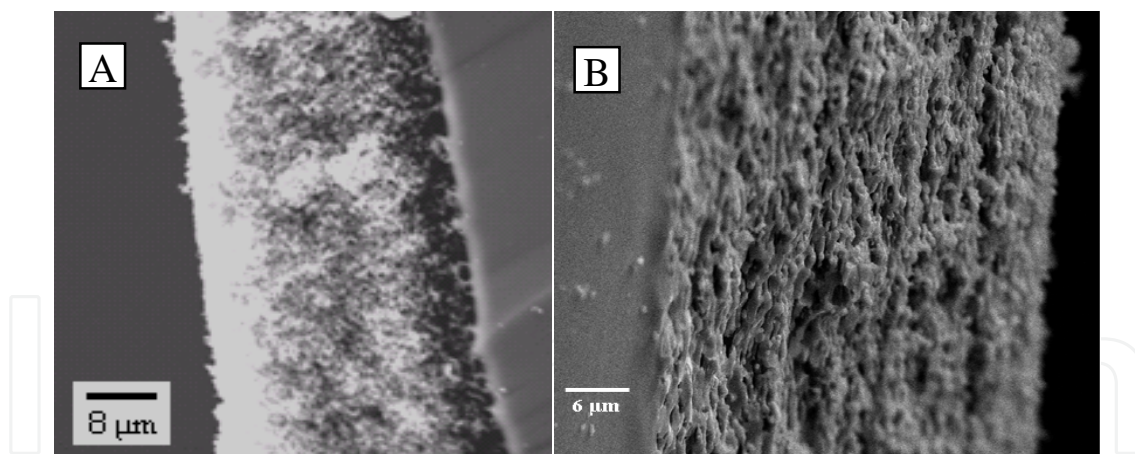


Fig. 5. The microscopic radial view of six multiple porous layers (A) and ten multiple porous layers (B) deposited at around  $1275 \pm 10^\circ\text{C}$  and  $1240 \pm 10^\circ\text{C}$ , respectively.

### 2.7 Composition of the solution of dopant precursors

Several preforms were made using various strength of  $\text{AlCl}_3 \cdot 6\text{H}_2\text{O}$ ,  $\text{YCl}_3 \cdot 6\text{H}_2\text{O}$ ,  $\text{LiNO}_3$  and  $\text{YbCl}_3 \cdot 6\text{H}_2\text{O}$  which maintain the suitable viscosity around 1.5 cP (Paul et al., 2010). The viscosity of the solution of the dopant precursors plays an important role to prevent the disturbances of thick porous layer. Such disturbance of thick highly porous medium occurs if the viscosity of the soaking solution is high. The viscosity of 1.5 cP of the solution is found to be most suitable for soaking of six as well as ten numbers of porous layers deposited at

1350±10°C, 1275±10°C and 1240±10°C, respectively. The effect of high viscosity of the doping solution gives rise to an accumulation of the deposited soot particles after solution soaking process due to generation of high viscous force within the pores along with loosing out of the soot layers from the inner surface during drying with inert gas as well as heating process.

### 2.8 Soaking, drying and heat treatment of solution impregnated porous layers

Solution soaking process was done for a period of 30-60 minutes (depending on the numbers of deposited porous layers) followed by drying with flow of N<sub>2</sub> gas for a period of 45-60 minutes under very low pressure (~0.5-1.0 Psig) as well as drying thermally by heating around 600-700°C for a period of 10 minutes with flow of O<sub>2</sub> at the rate of 500cc/min along with He flow at the rate of 75cc/min for elimination of the problem of any disturbances of the thick porous layer (50-75µm).

### 2.9 Dehydration

Dehydration step is very important to reduce OH content of the fabricated fiber. Dehydration of core layer is carried out at lower temperature range (600-700°C) in presence of Cl<sub>2</sub>, O<sub>2</sub> and He due to evaporation of LiCl from Li<sub>2</sub>O during dehydration as the equilibrium constant value of the chlorination of lithium oxide is very high (Fig. 6) derived from FactSage (Facility for the analysis of chemical thermodynamics) 5.5 thermo chemical software and database. Li<sub>2</sub>O plays an important role to make transparent glass-ceramic (Morimoto, 2004; Morimoto & Emem, 2004). The optical transparency of yttria-alumino silica based core glass has been lost; if more amount of lithium evaporate.

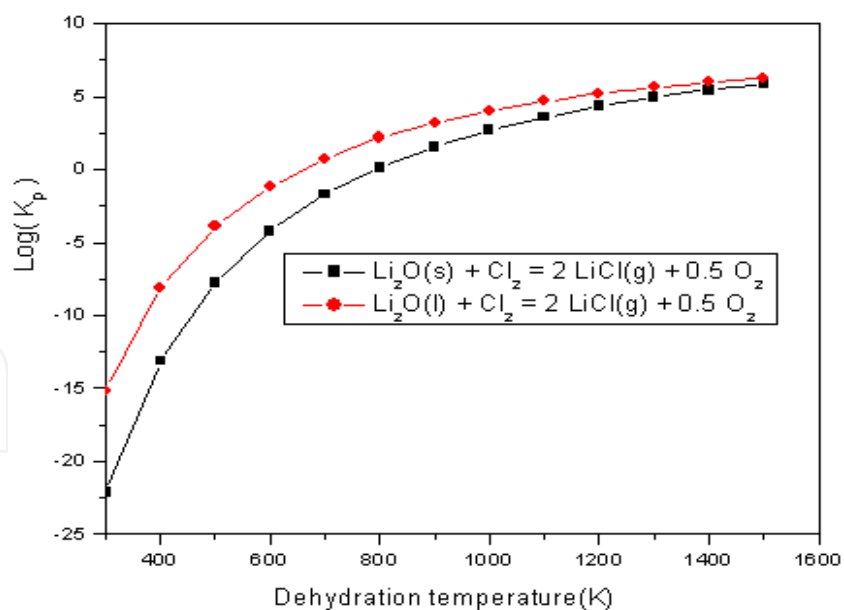


Fig. 6. Dehydration was done at low temperature around 700°C due to very high equilibrium constant of the evaporation of LiCl from Li<sub>2</sub>O

### 2.10 Sintering

At sintering stage, the heating temperature was increased gradually from 1300 to 1900°C by a step-wise increment of 100°C for elimination of the problem of formation of small bubbles

either at the core clad boundary or within the whole core region in presence of a mixture of O<sub>2</sub> and He having the ratio of He:O<sub>2</sub> (1:4 to 1:1). The disturbances of thick soot layer through the formation of bubbles either at the core-clad boundary or within the whole core region arises if the porous layers are not deposited at optimum deposition temperature. The formation of small bubbles also generate at the core-clad boundary during sintering of the thick soaked porous layers if the deposition temperature varies much from one layer to another layer specifically if the first layer deposited at higher temperature compared to the other layers or all the porous layers are deposited at higher temperature around 1500°C. The main reason arises due to lack of suitable porosity of the innermost layer compared to the other layers in terms of soaking ability of the dopant precursors for smooth sintering. In this case, the bubble formation occurs due to high viscosity mismatch between the inner and uppermost layers. During viscous sintering process, the upper layers get sintered at lower temperature compared to the innermost layer. As a result of it, small bubbles may generate during sintering as well as collapsing stage from the innermost un-sintered layer.

### 2.11 Collapsing process

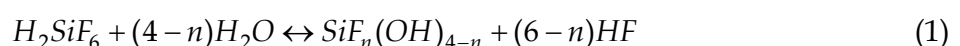
The collapsing was done in 3 steps. In the first step, partial collapsing occurs under high flow of O<sub>2</sub> around 250cc/min and He of 65cc/min at 15.0 psig to maintain circularity of the tube with burner speed of 40mm/min. In the second step the flow of O<sub>2</sub> was reduced to 75cc/min and He of 25cc/min at 5-6 psig with burner speed of 30mm/min. In the last pass, the flow of O<sub>2</sub> was increased to 125cc/min and He of 50 cc/min at 10 psig with burner speed of 15-20mm/min to maintain the perfect circularity of the large core after opening of the bypass line at the moment of final collapsing of one end.

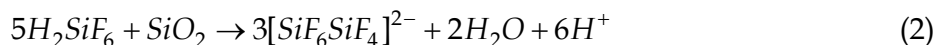
The solution doping technique followed by MCVD process using the above fabrication parameters provides homogeneous distribution of Al, Y, P and Yb ions as well as very uniform refractive index within the whole large core region of nano-engineering preform or fiber. The uniform doping levels within such large core optical fiber preform and refractive index profiles of corresponding optical fibers are also mentioned in this chapter.

### 2.12 Incorporation mechanism of fluorine into porous silica layer

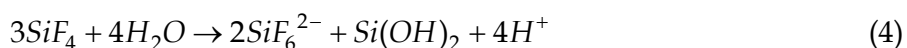
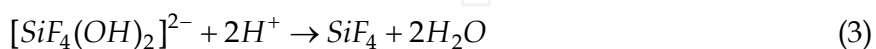
Fluorine was incorporated into porous layer through solution soaking process using H<sub>2</sub>SiF<sub>6</sub> (fluorosilicic acid) for 10-15 minutes. To prevent etching of porous layer in presence of F, the optimized 10-15% diluted H<sub>2</sub>SiF<sub>6</sub> was used. Furthermore, to avoid the formation of gelatinous precipitation with direct use of fluorosilicic acid into the alcoholic solution of chloride precursors, the double solution soaking process was performed for the incorporation of fluorine. Incorporation of fluorine into deposited porous silica surface was done based on the following mechanism.

The dilution of supersaturated fluorosilicic acid solution with water controls the incorporation of fluorine into the resulting porous silica matrix. An intermediate, hydrolyzed species, SiF<sub>n</sub>(OH)<sub>4-n</sub> (n < 4), will be formed by the reaction shown in Eq. (1) (Chou & Lee, 1994; Homma et al., 1993). These species present in the solution react with the porous silica substrate surface. The fluorine-containing siloxanes are subsequently formed, which adsorb onto the surface where condensation and bonding occurs between the oligomers and surface hydroxyl groups (Homma et al., 1993).





On the other hand, if we have used concentrated fluorosilicic acid, porous silica can be dissolved through formation of fluoro silicon complexes such as [SiF<sub>6</sub>.SiF<sub>4</sub>]<sup>2-</sup> shown in Eq. (2). The bridged fluoro silicon complex has electron deficient silicon because of the high electronegativity of the bonded fluorine, which create weak Si-F bonds. Such kind of bonds is very much prone to nucleophilic attack by water where fluorine ion (F<sup>-</sup>) combines with the proton to form hydrofluoric acid (HF). pH of the solution was adjusted properly where the high acidity of the solution allows protons to react with [SiF<sub>4</sub>(OH)<sub>2</sub>]<sup>2-</sup> to form SiF<sub>4</sub> and water through Eq. (3). Hydrolysis of SiF<sub>4</sub> will then yield hexa fluorosilicate anion, protons and silicic acid through Eq. (4) for incorporation of fluorine into porous silica layers.



A list of preforms having different doping levels along with fiber parameters are given in the following two tables.

Nano-preforms	Value of Al/Y (molar ratio)	Yb <sub>2</sub> O <sub>3</sub> (mol%)	P <sub>2</sub> O <sub>5</sub> (mol%)	BaO (mol%)	Fluorine (mol%)	Average particle size (nm)	Background loss at 1285nm (dB/Km)
NYb-1	20 :1	0.07	----	0.03	----	----	----
NYb-2	13 :1	0.12	----	0.05	----	----	----
NYb-3	6 :1	0.12	----	0.05	----	----	30
NYb-4	1.75 :1	0.14	----	0.07	----	20-30	75
NYb-5	1.75 :1	0.14	0.40	0.08	----	10-25	125
NYb-6	1.75 :1	0.14	0.50	0.07	----	25-50	450
NYb-7	1.75:1	0.14	0.60	0.08	0.25	25-60 3-5	2200
NYb-8	1.75:1	0.14	0.60	0.08	0.30	25-65 3-5	2400
NYb-9	1.75:1	0.14	----	0.08	0.25	6-10	40-50
NYb-10	1.7:1	0.10	0.20	----	----	10-15	45-60
IMNYb3	1.7:1	0.15	0.20	----	0.25	5-10	40-55
IMNYb4	1.7:1	0.15	0.20	----	0.25	5-10	45-60
IMNYb-12D	1.7:1	0.15	.20	---	0.25	5-10	40-65
IMNYb-12P	1.7:1	0.15	.20	---	0.25	5-10	45-60

Table 1. The doping levels of different nano-preforms evaluated by EPMA along with size of the particles and background loss of the fabricated nano-particles fibers.

Doping host	Fiber ID	No. of porous layers	Deposition temperature ( $\pm 10^\circ\text{C}$ )	CSA of the deposited tube ( $\text{mm}^2$ )	NA ( $\pm 0.02$ )	Cladding absorption at 976 nm (dB/m)	Core dia. ( $\mu\text{m}$ )
SiO <sub>2</sub> -Y <sub>2</sub> O <sub>3</sub> -Al <sub>2</sub> O <sub>3</sub> -P <sub>2</sub> O <sub>5</sub> -Yb <sub>2</sub> O <sub>3</sub>	NYb 4-NYb10	6	1350	82-85	0.09	5-10	15.0-20.0
SiO <sub>2</sub> -Y <sub>2</sub> O <sub>3</sub> -Al <sub>2</sub> O <sub>3</sub> -P <sub>2</sub> O <sub>5</sub> -Yb <sub>2</sub> O <sub>3</sub>	IMNYb-3, IMNYb-4	6	1275	58-60	0.09	5-10	22.0 $\pm$ 2.5
SiO <sub>2</sub> -Y <sub>2</sub> O <sub>3</sub> -Al <sub>2</sub> O <sub>3</sub> -P <sub>2</sub> O <sub>5</sub> -Yb <sub>2</sub> O <sub>3</sub>	IMNYb-12D & IMNYb-12P	10 under expanded condition	1240	58-60	0.09	5-10	32 $\pm$ 2.5

Table 2. Fabrication and fiber parameters of different large core nano-engineering fibers.

### 2.13 Thermal annealing process

The preform samples were annealed at different temperatures for appropriate time to find out the optimum temperature for the formation of nano-crystallites inside the silica glass matrix. After fabrication of preforms, we have made five circular sections of thickness around 1-1.5 mm having 10 mm diameter from each preform. Each section was heated in a temperature-controlled furnace of 1000, 1200, 1300, 1450 and 1650°C at the rate of 20°C/min and left for 3 hours once the temperature has been reached, to achieve the structural equilibrium, followed by the cooling to room temperature at a rate of 20°C/min. Depending on the glass composition the annealing step was optimized to obtain a highly transparent glass with the nano-sized crystallites distributed homogeneously in that, as well as a complete segregation of the RE ions into the nano-crystal site.

The diagram of annealing sequences of fiber preform samples heated at different temperatures in a closed furnace of Ar gas environment was shown in Fig. 7. The microscopic picture of the core region of fiber preform (NYb-7) with and without annealing was given in Fig. 8. The core glass of preform annealed at 1650°C and without annealing as shown in Fig. 8 becomes almost transparent. Whereas the preform annealed at 1450°C becomes highly opaque. This phenomena indicates that the nature of Yb<sub>2</sub>O<sub>3</sub> doped yttria-alumino silica host under thermal annealing at 1450°C becomes different than that of core glass matrix of preform samples without annealing and with annealing under heat treatment at 1650°C. The nature of such kind of glass was evaluated from XRD and TEM along with EDX as well as electron diffraction pattern analyses. The observation of the thermal annealing of preform samples at different temperatures is given in Table 3.

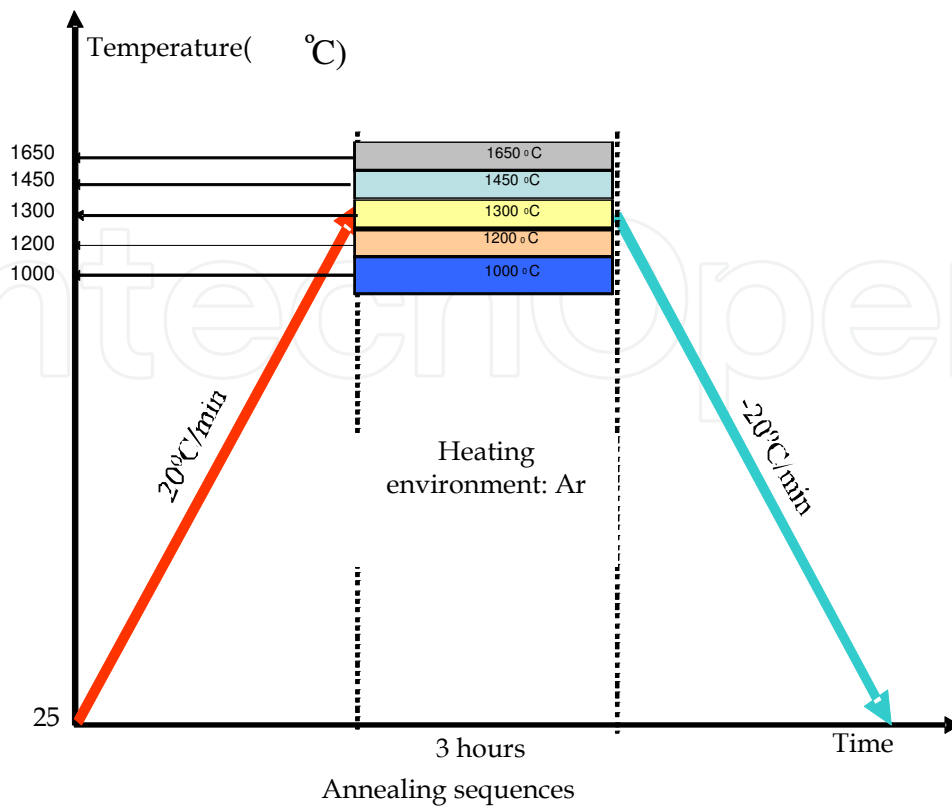


Fig. 7. The diagram of annealing sequences fiber preform samples heated at different temperatures in a closed furnace.

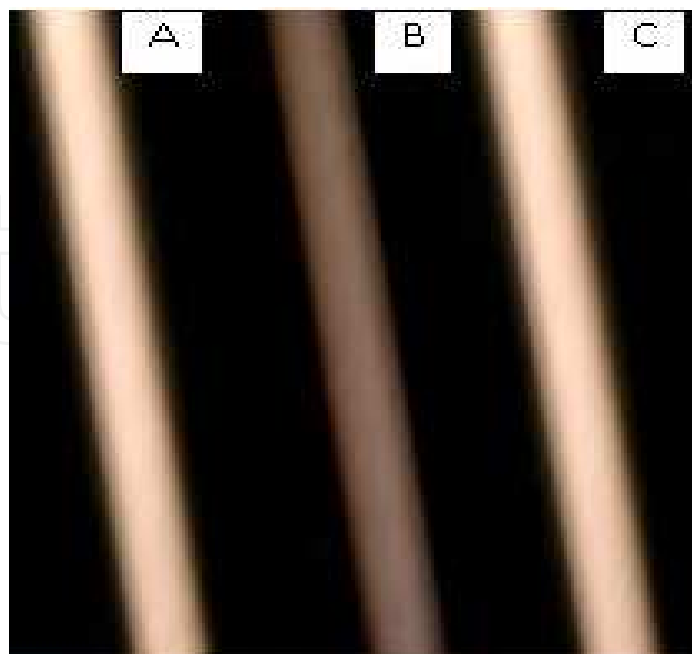


Fig. 8. Microscopic picture of the core region of preforms (A) Preform without annealing (B) Annealed at 1450°C for 3 hours (C) Annealed at 1650°C for 3 hours.

Sample numbers	Heating rates (°C/min)	Soaking period (hr)	Observation against thermal soaking temperature				
			1000°C	1200°C	1300°C	1450°C	1650°C
NYb-7 Preform	20	3	Transparent	DNP (slightly milky)	DNP (slightly milky)	CNP (strong milky)	(slightly milky) (No particles)
NYb-8 Preform (Fluorine doped)	20	3	Transparent	DNP (slightly milky)	DNP (slightly milky)	CNP (strong milky)	(slightly milky) (No Particles)

Table 3. Conditions and effect of thermal annealing of preform samples at different temperatures.

After that milling and polishing of the annealed preforms are done. Milling was done for removal of the silica mass equivalent to 1mm depth from one side of the preform. Preform was milled using ultrasonic machine. After milling, D-shaped fiber with low index polymer coated was drawn using fibre draw tower.

### 3. Material characterizations of the nano-engineering doping host

The material characterizations of nano-engineering doping host have been done at different stages from deposition of multiple porous layers to making of optical preforms through the following various techniques.

#### 3.1 Scanning electron microscopy (SEM) analyses of porous layers

Different soot parameters namely density, pore sizes, porosity, surface area and soot layer thickness have been evaluated for optimization of deposition temperature of multiple porous layers against the numbers of deposited layers to get uniform distribution of different co-dopants along the diameter of fabricated preforms. The soot density was found to be around 0.258 gm/cc at optimum deposition temperature regions namely  $1350 \pm 10^\circ\text{C}$ . The porosity of six numbers of porous layers deposited at  $1350 \pm 10^\circ\text{C}$  along radial direction was found to be 58% to 62% from innermost layer to outermost layer as described earlier in Fig 3. The reason behind the slight decrease in porosity is a consequence of partial sintering. Both scanning electron microscopy (SEM LEO, S430i, LEO, UK) and field emission scanning electron microscopy Supra 35VP (Carl Zeiss, Germany) images of soot layer samples were captured before and after solution doping shown in Fig. 9 to investigate the average pore sizes, their distribution and soot layer thickness. The average pore size was evaluated from SEM micrographs using Image analyzer and found to be 1.25-1.5 micron.

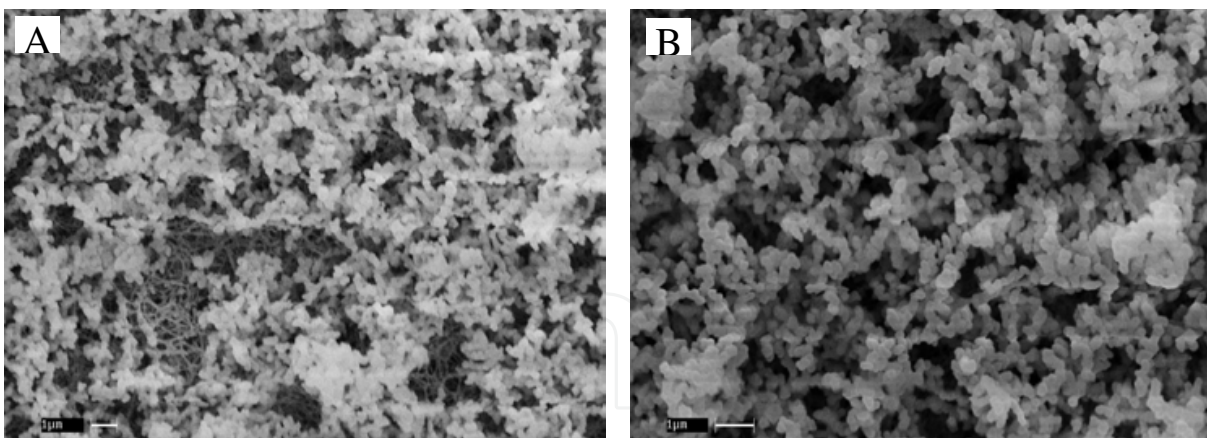


Fig. 9. SEM pictures of axial view of the porous layers (6 numbers) deposited at temperature around  $1350 \pm 10^\circ\text{C}$  (A) before (B) after solution soaking.

### 3.2 Atomic force microscopy (AFM) study

The technique which used for the analysis of porous silica layers is the Atomic Force Microscopy (AFM) Model: Multiview 3000 (Nanonics Imaging Ltd., Israel). AFM images are obtained by measurement of the force on a sharp tip (insulating or not) created by the proximity to the surface of the sample. This force is kept small and at constant level with a feedback mechanism. When the tip is moved sideways it will follow the surface contours. By this way, three dimensional images of the surface of the porous samples are obtained. A three-dimensional view and a corresponding cross section graph of the deposited porous surface shows a hillock profile with a dome height of  $3 \pm 0.25 \mu\text{m}$  and distance between dome tops  $4.0 \pm 1.0 \mu\text{m}$  shown in Fig. 10 and Fig. 11. Both circular and irregular shaped pores were observed, with diameters of  $3 \pm 1 \mu\text{m}$  and a pore-to pore distance of  $4.5 \pm 0.5 \mu\text{m}$ . The porosity of the deposited thick layer was determined as  $60 \pm 2.0\%$ .

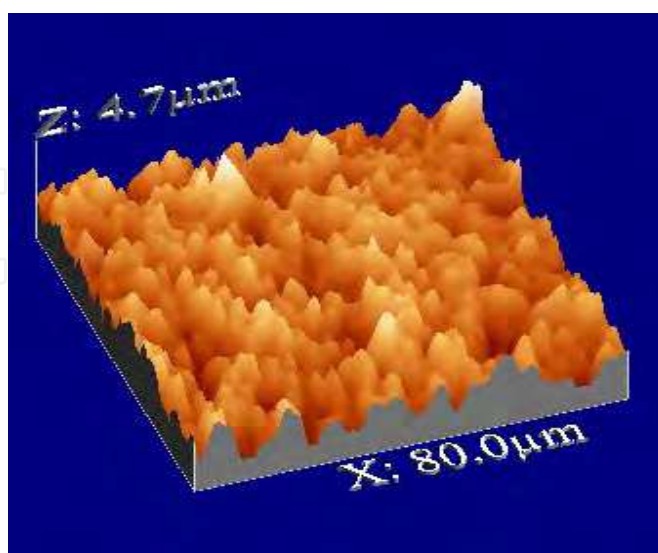


Fig. 10. A three dimensional AFM image of the surface of porous phospho-silica multi-layers.

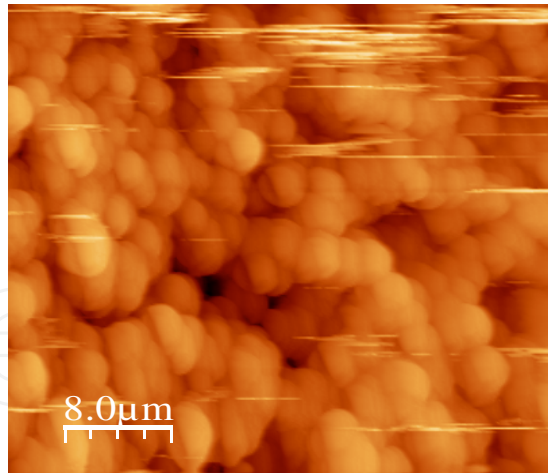


Fig. 11. A cross-sectional AFM image of the surface of porous phospho-silica multi-layers.

### 3.3 Differential thermal analyses (DTA) of the porous material

The determination of glass transition and crystallisation temperatures as well as melting temperature of such nano-engineering core glass material was also important for better understanding of the phenomena of phase separation as well as crystallisation mechanism with respect to the doping solution composition. Differential thermal analyser (DTA) Model: STA 409C (Netzsch, Germany) on samples ground to an average particle size of less than 25  $\mu\text{m}$  was prepared. In such case, unsintered oxide porous layer of composition  $\text{SiO}_2\text{-P}_2\text{O}_5\text{-Y}_2\text{O}_3\text{-Yb}_2\text{O}_3\text{-Li}_2\text{O-BaO}$  formed by MCVD process followed by solution doping technique (soaked with an alcoholic solution of  $\text{YbCl}_3 \cdot 6\text{H}_2\text{O}$ ,  $\text{YCl}_3 \cdot 6\text{H}_2\text{O}$ ,  $\text{AlCl}_3 \cdot 6\text{H}_2\text{O}$ ,  $\text{LiNO}_3$ ,  $\text{BaCl}_2 \cdot 2\text{H}_2\text{O}$ ) and after oxidation of the soot was removed from the inner surface of the silica tube and then ground to a powdered material for DTA. The DTA measurements were carried out using minimum about 30 mg of sample in a Pt crucible. Data for each run was automatically collected from the DTA apparatus. The glass transition and crystallization temperature of such type of glass was found to be around 985 and 1115°C respectively shown in Fig. 12. The exact melting temperature was not detected due to the temperature limitation of DTA upto 1450°C.

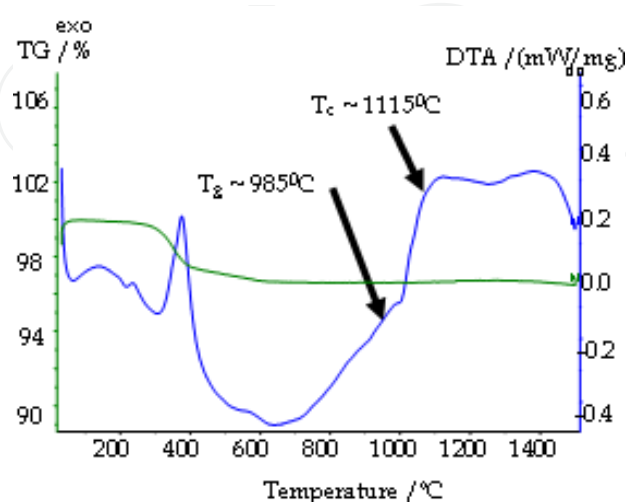


Fig. 12. Differential thermal analysis (DTA) curve of fluorinated  $\text{Yb}_2\text{O}_3$  doped silica soot.

### 3.4 Electron probe micro-analyses (EPMA)

The average dopant percentages in samples were measured by an electron probe microanalyser (EPMA) at University of Minnesota, Electron Microprobe Laboratory, USA. For this, around 3-4 mm of the preform sample was grounded and polished both sides. Finally EPMA of the polished preform samples of thickness 1-1.5 mm was done with the maximum spatial resolution of  $1\mu\text{m}$  after applying a thin graphite coating layer. Data of EPMA of preform samples were taken with a spatial gap of 30 micron within the whole core region shown in Fig. 13. The corresponding different dopant distribution of large core fiber preforms IM-NYb3 and IMNYb-12D are described in Fig. 14 and Fig. 15 respectively.

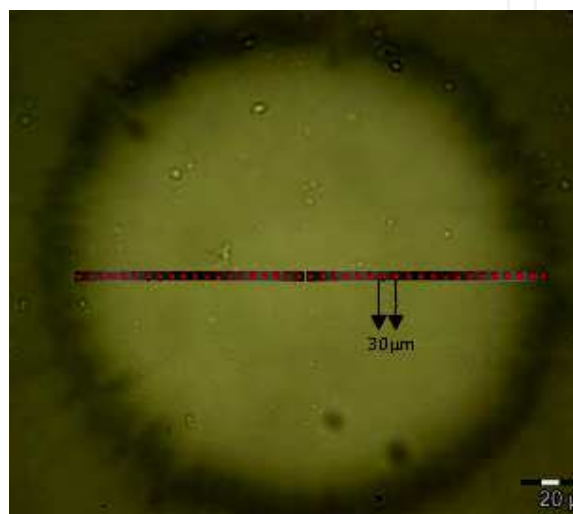


Fig. 13. Data of EPMA of preform samples taken with a spatial gap of  $30\mu\text{m}$  within the core region

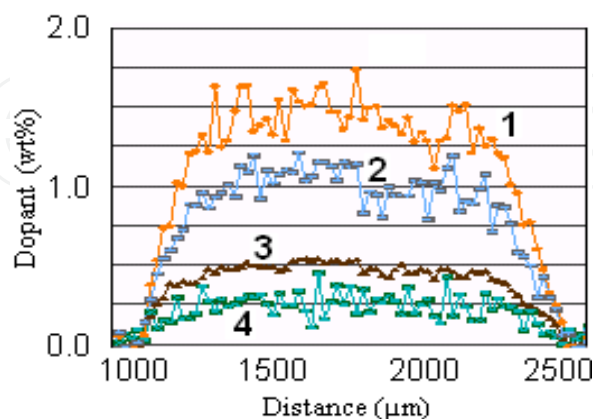


Fig. 14. Distributions of doping levels of  $\text{Al}_2\text{O}_3$  (1),  $\text{Y}_2\text{O}_3$  (2),  $\text{Yb}_2\text{O}_3$  (3) and F (4) within the core area of fiber preform (IM-NYb-3).

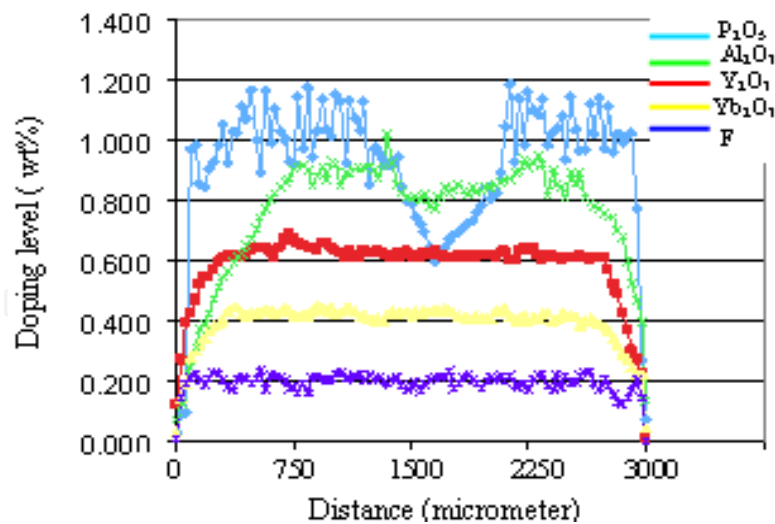


Fig. 15. Distributions of doping levels of  $\text{Al}_2\text{O}_3$  (1),  $\text{Y}_2\text{O}_3$  (2),  $\text{Yb}_2\text{O}_3$  (3) and F (4) within the core area of fiber preform (IMNYb-12D).

### 3.5 X-ray diffraction (XRD) study

To detect the exact crystalline phases formed during the heat treatment, X-ray diffraction (XRD) was performed on finely ground core glass specimens. The X-ray Patterns was collected using a powder diffractometer. X-ray diffraction spectra were extracted from the raw 2-dimensional data using the Fit2D program (Hammersley et al., 1996). Spectra were collected on nano-engineering preform sample (NYb-8) annealed at different temperatures shown in Fig. 16. The calibration of the distance between the sample and the detector was carried out by using a  $\text{LaB}_6$  sample (NIST SRM660). Only the samples annealed at  $1450^\circ\text{C}$  present crystalline peaks. The preform annealed at other temperatures does not show any characteristics diffraction peak of Yb:YAG crystals. The exact diffraction peaks of Yb:YAG crystals embedded in silica matrix is found to be  $33.43^\circ$ (a),  $46.606^\circ$ (b),  $56.34^\circ$ (c) when annealed at  $1450^\circ\text{C}$  in comparison to the exact characteristics peaks at  $33.064^\circ$ ,  $46.183^\circ$  and  $55.732^\circ$  given in Joint Committee on Powder Diffraction Standards (JCPDS-38-0222) (Joint Committee on Powder Diffraction Standards, data file. 38-0222) and also observed by W. Yusong et al. (Yusong et al., 2007)

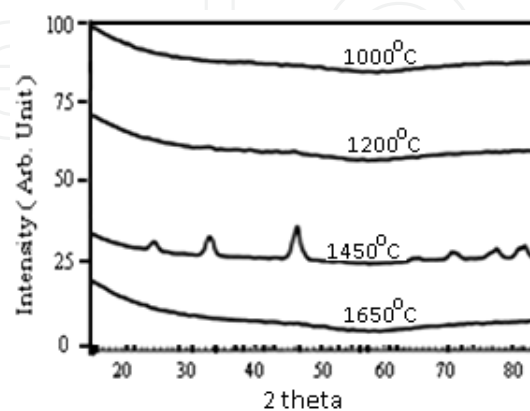


Fig. 16. X-ray diffraction spectra of the doped region of preform NYb-8 annealed at four different temperatures for 3 hours and different crystalline peaks developed for sample annealed at  $1450^\circ\text{C}$ .

### 3.6 X-ray absorption spectroscopy

Distribution of Yb ions in the glass preform was also determined by the fluorescence yield of the Yb L $\alpha$  line given in Fig. 17. The vertical line marks the point where the XAS measurement has been carried out. The following figures shows a typical distribution profile of Yb ions in the preform measured by X-ray fluorescence: these permits to determine the size of the Yb-doped zone that resulted to be of about 1.5 mm. The vertical bars indicate the point where the EXAFS spectra will be carried out that was chosed to be in the middle of the fibre core.

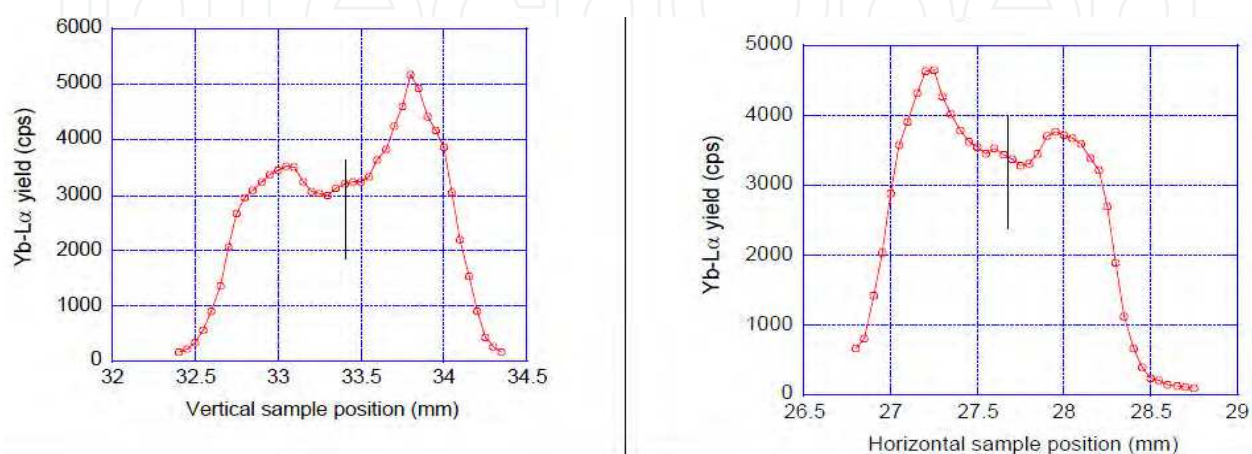


Fig. 17. The fluorescence yield of the Yb L $\alpha$  line of nano-engineering preform (NYb-5). The vertical line marks the point where the XAS measurement has been carried out.

### 3.7 High resolution transmission electron microscopy (HRTEM) with electron diffraction pattern and EDX analyses

High resolution transmission electron microscope (HTEM) Model:Tecnai G2 30ST (FEI Company, USA) images of preform samples were used to study the core glass morphology using LaB<sub>6</sub> emitter. The TEM specimens were mechanically polished and dimpled to thickness of about 10  $\mu$ m. The final thinning of the samples to electron transparency was carried out using an Ar-ion mill. To evaluate the composition of phase-separated particles the electron beam was focused on the particles and then focused in an area outside of the particles, when the energy dispersive X-ray analyses (EDX) data were taken. The nature of the particles was evaluated from their electron diffraction pattern. TEM picture along with electron diffraction pattern of Yb<sub>2</sub>O<sub>3</sub> doped nano-crystalline glass based optical fiber preform (NYb-4) after thermal annealing at 1450°C temperature was shown in Fig. 18.

## 4. Effect of suitable dopant levels and thermal annealing on formation of crystalline nano-particles

Study on the effect of suitable dopant levels specifically the ratio of Al:Y and thermal annealing on formation of crystalline nano-particles within the core region of optical fiber preform samples were done through TEM along with electron diffraction pattern, EDX and XRD analyses. For this purpose several Yb<sub>2</sub>O<sub>3</sub> doped large core preforms (listed in table 1) were fabricated with varying Al:Y ratio from 20:1 to 1.75:1 and other co-dopants, in order to study the dependence of glass composition on the formation of nano-crystalline particles. All co-dopants, except for P are incorporated in the structure through solution doping process.

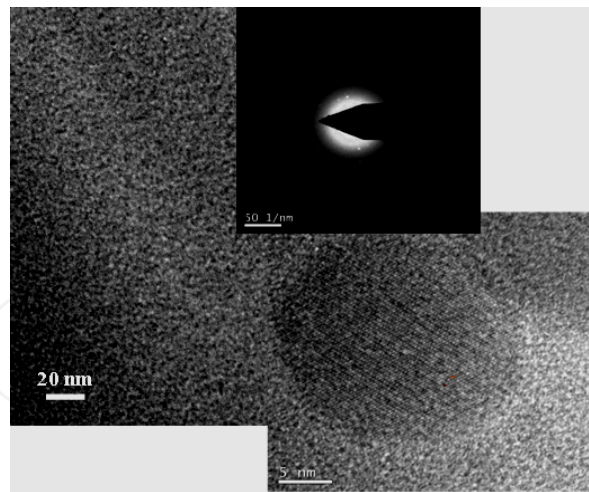


Fig. 18. TEM picture along with electron diffraction pattern as well as  $\text{Yb}_2\text{O}_3$  doped crystalline nano-particles developed within yttria-alumino silicate glass of optical fiber preform (NYb-4) after thermal annealing at  $1450^\circ\text{C}$

Two important parameters were involved for formation of  $\text{Yb}_2\text{O}_3$  doped phase-separated yttria alumino-silicate nano-crystalline host. First, the doping ratio of Al:Y and second, suitable thermal treatment of the fabricated preform. The optimised thermal annealing conditions of preforms were identified to get  $\text{Yb}_2\text{O}_3$  doped phase-separated nano-crystalline particles of composition Yb:YAG. The strength of dopant precursors of Y and Al within the doping solution was varied gradually from preform NYb-1 to NYb-4 to get the initial condition for formation of the phase-separated nano-particles within the preform samples. The ratio of Al:Y within the fiber preform samples were calculated from EPMA results. No-phase-separated particles were developed within the preforms of NYb-1, NYb-2 and NYb-3 under any thermal annealing conditions when the ratio of Al:Y varied from 20:1 to 6:1. Fig. 19 shows the TEM image of preform NYb-2 having Al:Y ratio of 13:1 and annealed at temperature of  $1300^\circ\text{C}$  with no evidence of nano-particle formation. However, the preform NYb-4 having Al:Y ratio of 1.75:1 shows phase-separated nano-particles under thermal annealing at  $1300^\circ\text{C}$  for 3 hours (Fig. 20). The formula of YAG crystal is  $\text{Y}_3\text{Al}_5\text{O}_{12}$  where the ratio of Al:Y is around 1.7. Here the role of Al and Y at that ratio favours the formation of YAG crystals stoichiometrically. Higher than this ratio, excess Al prevents the formation of phase-separation which does not enter within the immiscibility region of yttria alumino silicate glass.

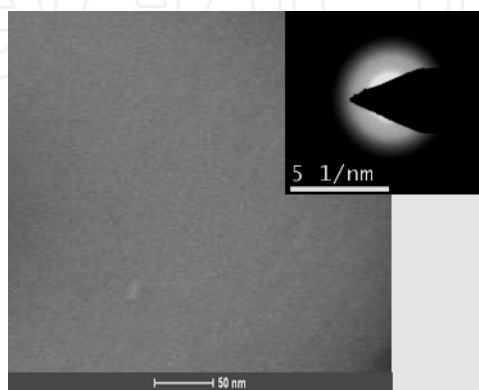


Fig. 19. TEM image of the doped area of preform NYb-2 annealed thermally at around  $1300^\circ\text{C}$  for 3 hours.

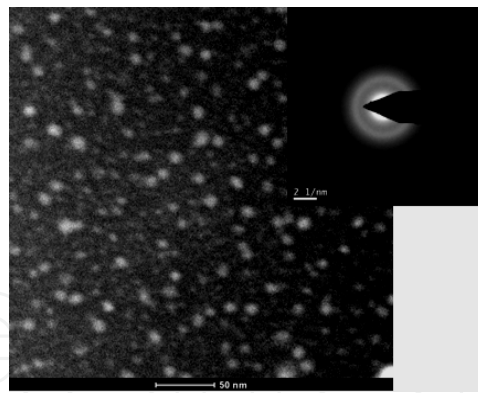


Fig. 20. TEM image of the doped area of preform NYb-4 annealed thermally at around 1300°C for 3 hours along with electron diffraction pattern.

On the other hand preform NYb-4 when annealed at 1000°C for 3 hours does not form any phase-separated particles as shown in Fig. 21. The formation of phase-separated amorphous particles started when the preform samples NYb-5 and NYb-6 annealed at 1200°C, as shown in Fig. 22 and Fig. 23.

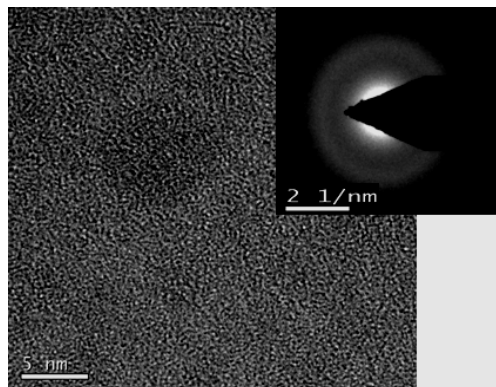


Fig. 21. TEM image of doped area of preform NYb-4 annealed thermally at around 1000°C.

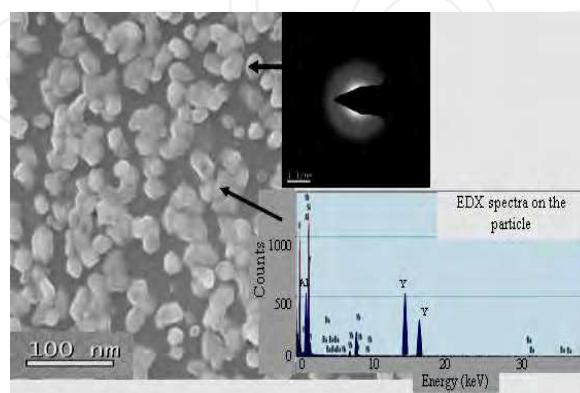


Fig. 22 . TEM image of doped area of preform NYb-5 annealed at 1200°C containing 0.40 mol%  $\text{P}_2\text{O}_5$  along with electron diffraction pattern and EDX spectra.

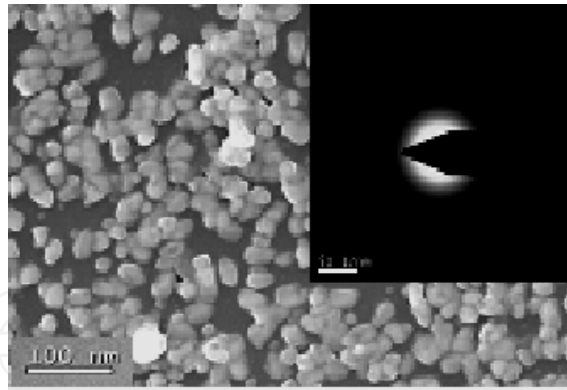


Fig. 23. TEM image of doped area of preform NYb-6 annealed at 1200°C containing 0.50 mol% of  $P_2O_5$  along with electron diffraction pattern.

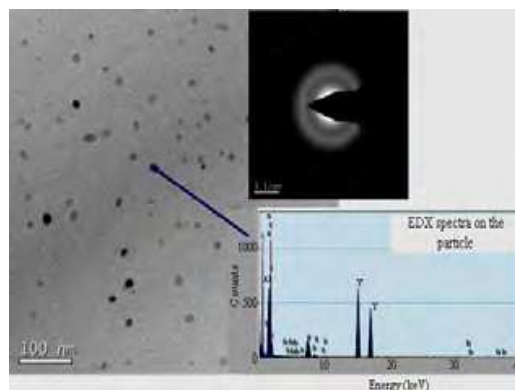


Fig. 24. TEM image of the doped area of preform NP-5 annealed at 1300°C containing 0.40 mol% of  $P_2O_5$  along with electron diffraction pattern and EDX spectra.

At this annealing temperature the nano-particles which have grown together resulted in an interconnected nano-structure. The electron diffraction pattern shows the formation of amorphous phase (inset Fig. 22 and Fig. 23). When the same preform samples heated at around 1300°C, the nano-particles are separated from each other and mostly single isolated particles distributed uniformly in the core glass matrix were observed, as shown in Fig. 24 and Fig. 25. The TEM pictures shown in Fig. 22 to Fig. 25 for heat treated samples under 1200 and 1300°C are to study the effect of annealing temperature on the formation of phase-separated particles along with its nature. The isolated particles are not YAG nano-crystallites. The particles are  $Yb_2O_3$  doped phase-separated yttria-rich alumino-silicate nano-particles evaluated from their corresponding EDX data.

Further annealing of the preform at around 1450°C, all the phase-separated particles became crystalline. The electron diffraction pattern as shown in the inset of Fig. 26 and Fig. 27 demonstrates that the particles are crystalline in nature.

High resolution micrographs (Fig. 28) were extracted from the previous TEM pictures of preforms NYb-5 and NYb-6 after thermal annealing at 1450°C for 3 hours, which show the crystalline nano-structure of less than 20 nm in size and surrounded by the amorphous  $SiO_2$  matrix. At the crystalline orientation the phase contrast allows to differentiate lattice plans of  $\sim 0.3$ nm separation. This matches with the value reported by Jian-Cheng Chen (Chen, 2006). The lattice planes show that the original nano-crystals have combined to form a continuous crystalline lattice. Absence of grain boundaries within the crystalline phase

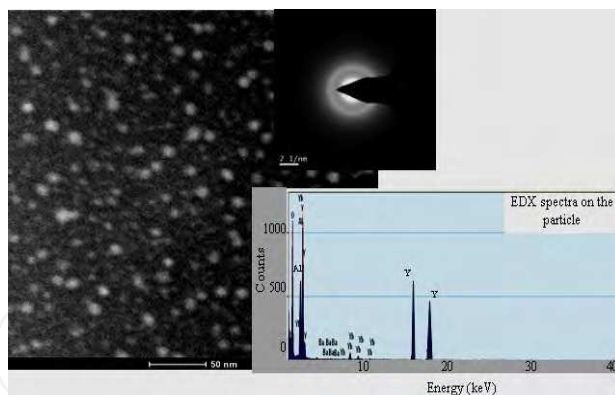


Fig. 25. TEM image of the doped area of preform NYb-6 annealed at 1300°C containing 0.50 mol% of  $\text{P}_2\text{O}_5$  along with electron diffraction pattern and EDX spectra.

might be due to the agglomeration of independent nano-crystals. Here, two nano-crystals are separated by a layer of amorphous phase. The interconnection of the phase-separated particles developed during thermal annealing at 1450°C leads to the growth of a nano-crystalline structure shown in Fig. 28. All the particles were observed to be near round shape. The driving force behind the roundish morphology and interconnection of individual nano-crystals is due to the lowering of surface energy of the connected crystal network over individual nano-crystals.

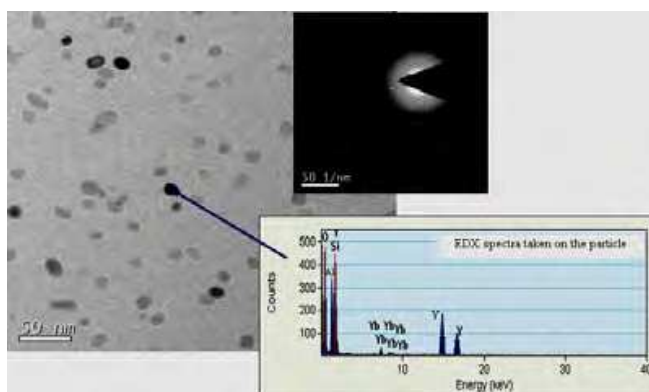


Fig. 26. TEM image of the doped area of preform NYb-5 annealed at 1450°C containing 0.40 mol% of  $\text{P}_2\text{O}_5$  along with electron diffraction pattern and EDX spectra.

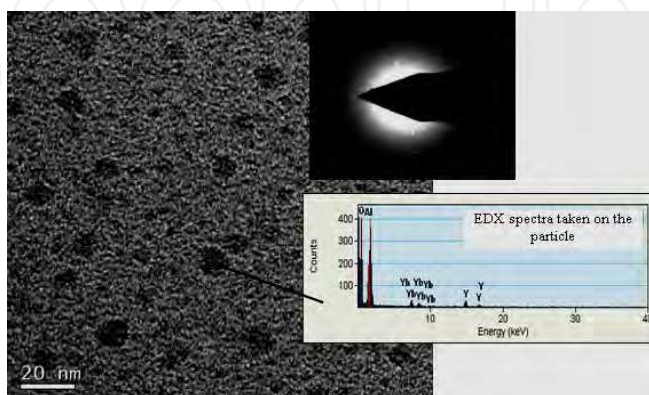


Fig. 27. TEM image of the doped area of preform NP-6 annealed at 1450°C containing 0.50 mol% of  $\text{P}_2\text{O}_5$  along with electron diffraction pattern and EDX spectra.

The composition of such phase-separated crystalline particles was evaluated by comparing their energy dispersive X-ray analyses (EDX) data, taken from directly on the crystal particles and from the areas of outside the particles shown in Fig. 28. The EDX spectra taken from the crystal particles detected as Si, Al, O, Yb and Y signals, whereas the EDX data taken from the areas outside the particles detected Si, Al and O without Yb and Y. Si signal appear as the crystals are embedded with SiO<sub>2</sub>. The dopant concentration of nano-crystallites with respect to the silica matrix was evaluated from EDX curve and shown in Fig. 28. The evaluated data consists of 13.0 atom% of Al, 0.02 atom% of Yb, 8.0 atom % of Y and 34.0 atom% of O. The doping level of the formation of Yb:YAG crystals within fiber preform sample (NYb-5) is 0.02 atom%. Such compositional analyses indicates that the phase-separated crystalline nano-particles were Yb:YAG crystals dispersed into the silica glass matrix.

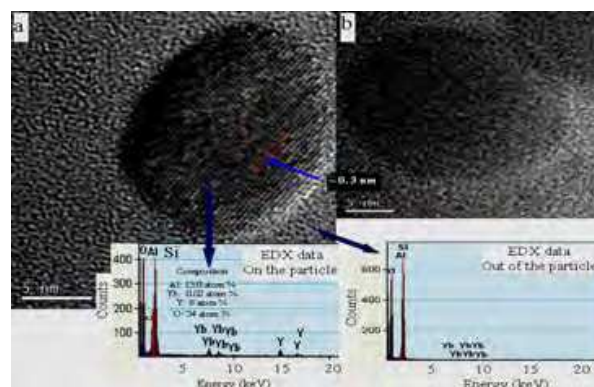
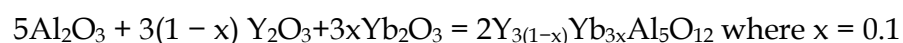


Fig. 28. HRTEM image showing the lattice plan of the crystalline nano-particles developed within the doped region of preforms (a) NYb-5 and (b) NYb-6 annealed at 1450°C for 3 hours along with EDX spectra taken on and out of the particles.

The nature of the glass host was evaluated from X-ray diffraction spectra of the doped region of preform (NYb-5) annealed at 1300°C and 1450°C for 3 hours shown in Fig. 29. The vertical lines correspond to YAG phase. The preform annealed at 1300°C does not show any characteristics diffraction peak of Yb:YAG crystals. The exact diffraction peaks corresponding to the lattice plan of 420, 611 and 633 of Yb:YAG crystals embedded in silica matrix is found to be 33.43, 46.606, 56.34 respectively when annealed at 1450°C in comparison to the exact characteristics peaks at 33.064, 46.183 and 55.732 respectively described in Joint Committee on Powder Diffraction Standards (JCPDS-38-0222) (Joint Committee on Powder Diffraction Standards, data file. 38-0222) and also observed by W. Yusong et. Al (Yusong et al., 2007). Such a small variation occurs as Yb:YAG crystals are embedded in silica glass based matrix and not in a perfectly Yb:YAG ceramic state.

Generally the formation of such type of Yb:YAG crystals in bulk glass samples occurs by the following way :



Similar type of reaction may takes place within yttria-alumino-silicate core glass matrix of optical fiber preform where the substitution of Y<sup>3+</sup> by Yb<sup>3+</sup> occurs due to their same valence state as well as similar ionic radius. On the other hand, Si<sup>4+</sup> may substitute for Al<sup>3+</sup> or it may sit at an interstitial position since the ionic radii of Si<sup>4+</sup> are 0.040 and 0.054 nm, and the ionic radii of Al<sup>3+</sup> are 0.053 and 0.068 nm, if their coordination numbers are 4 or 6, respectively<sup>59</sup>.

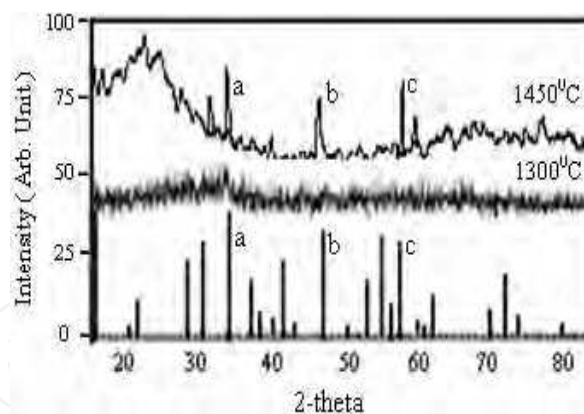


Fig. 29. X-ray diffraction spectra of the doped region of preform NYb-5 annealed at 1300°C and 1450°C for 3 hours. The vertical lines corresponds to YAG phase.

The possibility of sitting  $\text{Si}^{4+}$  to an interstitial site can be neglected as the large strain and higher number of vacancies per Si in an interstitial location will make the energies required for the incorporation very high. We have not observed formation of  $\text{Yb}_2\text{O}_3$  doped mullite crystals within the preform samples due to the large difference in ionic radii of  $\text{Al}^{3+}$  and  $\text{Yb}^{3+}$  ( $\sim 0.05$  nm) which results in lattice strain to restricts the formation of a solid solution comparable to mullite.

When the preform samples annealed above 1600°C, the crystalline behaviour of the particles were destroyed and most of the particles disappear, as shown in Fig. 30. This may be due to reaching of the melting temperature of the glass. The glass transition and crystallization temperature of such type of glass was found to be around 985 and 1115°C respectively as mentioned earlier in Fig. 12. The exact melting temperature was not detected due to the maximum limit of 1400°C temperature of our DTA apparatus. However from the fabrication point of view, the sintering of deposited layer starts around 1600°C which correspond to the melting temperature of the doped porous layer.

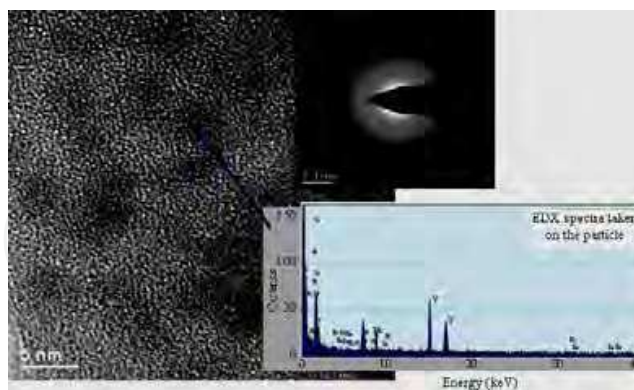


Fig. 30. TEM image of the doped region of preform NYb-5 annealed at 1600°C along with electron diffraction pattern and EDX spectra.

## 5. Effect of $\text{P}_2\text{O}_5$ and fluorine on formation of nano-particles within the core of preforms and fibers

The effect of phosphorous and fluorine doping on formation of  $\text{Yb}_2\text{O}_3$  doped nano-crystalline particles within silica glass matrix was studied through high-resolution TEM

analyses. The core glass remains transparent after annealing at 1000 and 1600°C. On the other hand, when annealed at 1450°C, the core region becomes slightly opaque which indicates the formation of phase-separated nano-crystalline particles in the preform sample. Fig. 26 and Fig. 27 shows the TEM pictures of two preform sections ( NYb-5 and NYb-6 ) having different content of  $P_2O_5$  for investigation of the effect of  $P_2O_5$  on the size and nature of the nano-particles. The maximum particle size in high  $P_2O_5$  content (0.50 mol%) core glass preform, NP-6, was found to be larger compared to the preform NYb-5 containing less  $P_2O_5$  content (0.40 mole%) in the core.

Increasing the  $P_2O_5$  content in glass accelerate the growth of formation of phase separated particles upon heating through thermal perturbation, where  $P_2O_5$  serves as a nucleating agent owing to the higher field strength difference ( $>0.31$ ) between  $Si^{4+}$  and  $P^{5+}$  (Tomazawa & Doremus, 1979). We have taken several TEM pictures from different sections of the core region of samples NYb-5 and NYb-6 to find out the variation of particle sizes. A wide variation from 10-25 nm and 25-50 nm in particle sizes were observed from the preform samples NYb-5 and NYb-6 respectively. The size of the nano-particles increased with increasing of the  $P_2O_5$  content. At the ratio of 20:1, 13:1 and 6:1 within the glass matrix formation of any nano-particles within the doped region of optical fiber preform under annealing upto the temperature of 1600°C does not occur.

The effect of fluorine on the formation of  $Yb_2O_3$  doped crystalline nano-particles within the preform samples NYb-7 and NYb-8 after thermal annealing at 1450°C are shown in Fig. 31 and Fig. 32 respectively. Here fluorine was incorporated using 10-15% fluorosilicic acid. Both preforms contain the same doping levels of  $P_2O_5$  (0.60 mol%). The doping level of fluorine content was measured by electron probe microanalyses (EPMA). The distribution profile of fluorine content along the diameter of core region of two fiber preform NYb-7 and NYb-8 was shown in Fig. 33. The average doping level of fluorine in preforms NYb-7 and NYb-8 was found to be 0.25 and 0.3 mole%. The spherical particles in Fig. 31 and 32 show bimodal size distribution. The large particles are of the order of 60 nm and the smaller ones are of the order of 3-5 nm. In addition, a very dense distribution of nano-particles (~2-10 nm size) was detected which are rich in high atomic number elements of Yb and Y. This was confirmed from the corresponding EDX spectra taken in the region of densely distributed nano-particles of preform NYb-7 which shows strong signals of Yb and Y.

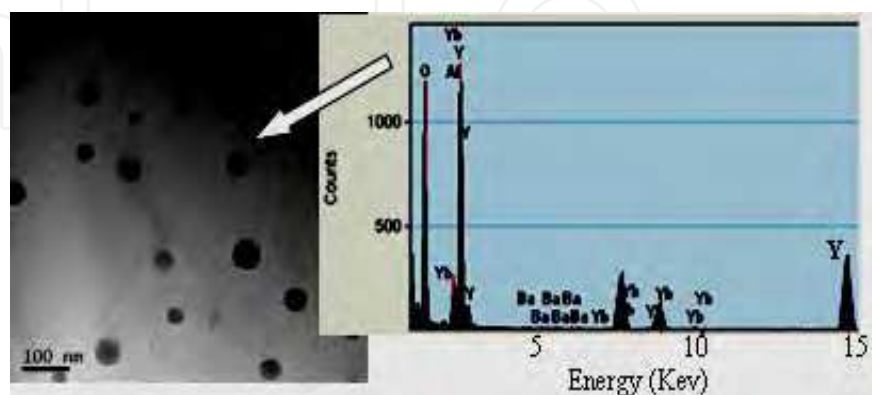


Fig. 31. TEM image and EDX spectra of the area of a dense distribution of nano-particles (2-10 nm) of preform NYb-7 annealed at 1450°C containing 0.6 mol% of  $P_2O_5$  and 0.25 mol% of fluorine.

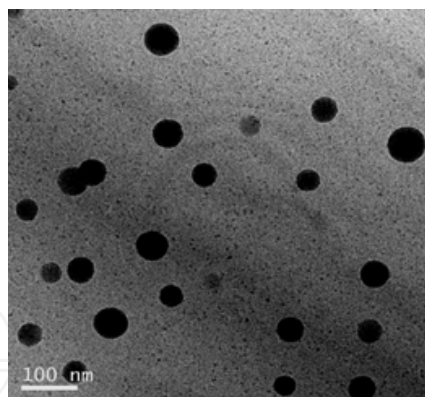


Fig. 32. TEM image of the area of preform NYb-8 annealed at 1450°C containing 0.6 mol% of P<sub>2</sub>O<sub>5</sub> and 0.30 mol% of fluorine

The doping of fluorine in yttria-alumino silicate glass composition may have a dramatic effect on the nucleation and crystallisation behaviour of the glass contributing to the bimodal size distribution. This effect was not only a result of the stoichiometric considerations of crystal formation but also of the network disrupting role of fluorine within a glass network. Here fluorine may act as a nucleating agent, promoting crystallization of Yb<sub>2</sub>O<sub>3</sub> doped YAG crystals within the silica glass matrix and also serves as a facilitator of the kinetics of crystallization through rearrangement of the glass network. The non-bridging oxygens preferentially bond to the silicon atoms present, thereby preventing the formation of silicon-fluorine bonds and the formation of volatile SiF<sub>4</sub>. In such glass, P and F may play a different kind of nucleation as well as crystallization phenomenon for the formation of observed bimodal size distribution.

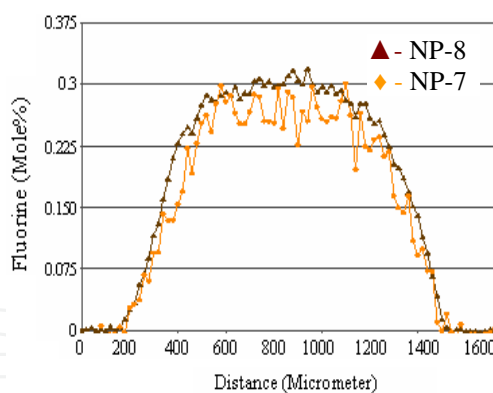


Fig. 33. Distribution profile of fluorine along diameter of two preforms NYb-7 and NYb-8.

The preform sample NYb-9, which contains 0.25 mol% F and no P<sub>2</sub>O<sub>5</sub>, after thermal annealing at 1450°C shows uniform distribution of crystalline nano-particles (Fig. 34) having sizes around 6-10 nm. HRTEM image of the black dots of doped area of preform (NYb-9) shows the formation of the nano-crystalline particles of Yb:YAG. The corresponding electron diffraction pattern shows the crystalline behaviour of the particles. The HRTEM picture clearly shows the crystalline plan of Yb:YAG crystals having 0.3 nm separation of lattice plans. The exact composition of the crystalline nano-particles was evaluated from the corresponding EDX spectra. The evaluated data shows 15.0 atom% of Al, 0.02 atom% of Yb, 9.0 atom% of Y and 36.0 atom% of O.

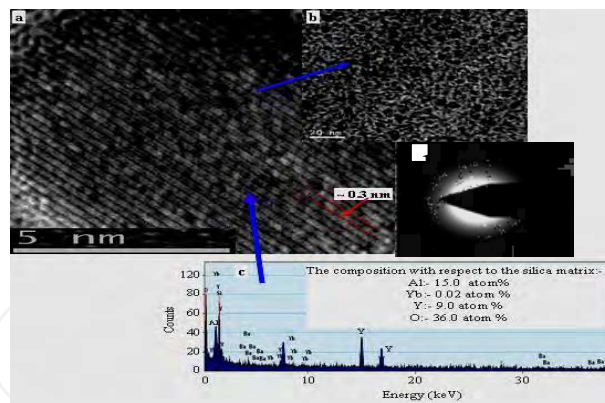


Fig. 34. HRTEM image of the doped area of preform NYb-9 annealed at 1450°C containing 0.25 mol% of fluorine showing (a) the nano-crystalline particles of Yb:YAG along with (c) EDX curve and (d) electron diffraction spectra.

## 6. Nature and sizes of the particles of Yb<sub>2</sub>O<sub>3</sub> doped nano-engineering fibers

Nature and sizes of the particles of nano-engineering fiber was evaluated from HRTEM analyses along with EDX and electron diffraction pattern. To make the TEM analyses of optical fiber samples first, fiber coating was removed. After that fiber was crashed in two different marble mortars and ground to fine powder. The glass powder was dispersed in acetone liquid. Cu saver was rinsed into the liquid and took out. After drying, the glass powder was stucked on the surface of the saver. The Cu saver was put under TEM to check the individual small particles by EDX. Nature and sizes of the particles of nano-engineering fiber was evaluated from HRTEM analyses along with EDX and electron diffraction pattern. The small phase-separated nano-particles within the doped core region of optical fiber NYb-9 was observed under TEM analyses shown in Fig. 35.

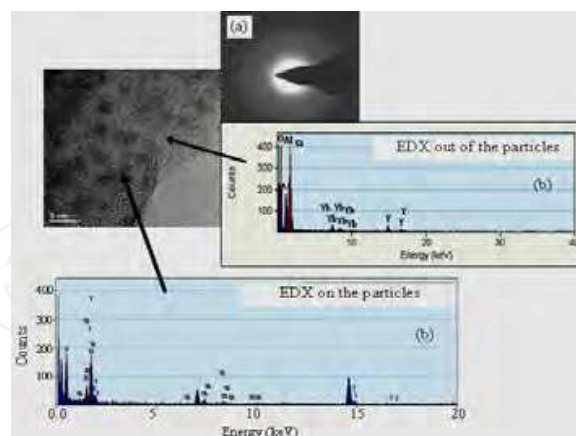


Fig. 35. TEM analyses of Yb-doped nano-particle silica optical fiber sample NYb-9 (a) Electron diffraction pattern and (b) EDX spectra on and out of the particles.

The size of the particles of the fiber core region occurs within 5.0-8.0 nm region. The EDX spectra shows that both phase-separated and non-phase separated regions contain Al, Y and Yb. However the intensity related to Y and Yb in phase-separated particles becomes very much larger than the non-phase-separated particles. On the other hand, the intensity related to Al in phase-separated particles becomes lower than that of non-phase-separated particles.

Such analysis indicates that most of ytterbium is located in the phase-separated yttria-rich region compared to Al dominated non-phase separated region. The nature of the phase-separated particles is found to be non-crystalline confirmed from their electron diffraction pattern. Such TEM analyses confirm the presence of Yb<sub>2</sub>O<sub>3</sub> doped phase-separated yttria-rich alumino-silicate amorphous particles. The corresponding EDX spectra indicates the presence of two different kind of Yb ions showing different surrounding environments. Fig. 35 confirm that the crystalline nano-particles initially formed in the preform (NYb-9) annealed at 1450°C was maintained within the fiber samples after drawing above 1900°C but nature of the particles changed from crystalline to amorphous state.

Here both P<sub>2</sub>O<sub>5</sub> and F serve as a nucleating agent to induce phase-separation in bulk silica glass matrix. We have studied the effect of P<sub>2</sub>O<sub>5</sub>, F and both on formation of YAG crystals within the fiber preform sample systematically. Both P<sub>2</sub>O<sub>5</sub> and F are important from view point of phase-separation phenomena to induce the formation of Yb:YAG crystals within silica glass matrix. On the other hand, incorporation of P<sub>2</sub>O<sub>5</sub> reduces the PD phenomena of the Yb<sub>2</sub>O<sub>3</sub> doped fiber laser. Fluorine incorporation into the doping host is also important as it reduces the refractive index of silica glass. As a result, incorporation of fluorine helps to maintain the required refractive index difference around 0.002-0.0025 with incorporation of larger content of Y and Al in order to achieve the ideal parameter of large mode area Yb<sub>2</sub>O<sub>3</sub> doped fiber for use as high power fiber laser with good lasing efficiency and beam quality. In this research work fluorine is found to be the most important as we are able to maintain the whole particles within 5-8 nm range in order to achieve the low background loss of the fiber within 40-50 dB/Km at wavelength 1285 nm. The details spectroscopic and lasing characteristics of Yb-doped nano-particles fibers drawn from the nano-crystalline preforms were mentioned earlier.

The formation of these nano-particles can be explained in terms of the phase separation phenomena and crystal growth mechanism, which normally occur in bulk silica based glass. Growth of Yb<sub>2</sub>O<sub>3</sub> doped nano-crystallites was based on the metastable nature of yttria-alumino silicate glass and will transform to the stable crystalline state, if enough thermal energy is available which occurs by a two step nucleation and crystal growth process (Varshneya, 1994; Rawson, 1967). As RE doped yttria-alumino silicate glass is heated, the viscosity decreases which in fact increases the tendency for structural rearrangement and crystallization. When the temperature was increased high enough (above 1350°C), crystal nuclei begin to form. The nuclei are the tiny regions in the glass structure. As the temperature was further increased, the rate of nuclei formation, or nucleation, increased and reached to a maximum at around 1450-1500°C, depending on the composition. At higher temperatures, additional thermal energy causes the nuclei to grow by crystal growth mechanisms. The rate of crystal growth increases with increasing temperature from 1450°C to a maximum of 1575°C and then the rate decreases to zero at the liquidous temperature around 1600°C. At temperature above 1600°C most of the particles disappears with destruction of their crystalline behaviour. Here, P<sub>2</sub>O<sub>5</sub> serves as a nucleating agent for promoting the phase-separation phenomena along with the crystallization. Both Y<sub>2</sub>O<sub>3</sub> and Al<sub>2</sub>O<sub>3</sub> serve as a formation of crystalline host of composition Y<sub>3</sub>Al<sub>5</sub>O<sub>12</sub>. The Li<sub>2</sub>O helps formation of glass-ceramic based material increasing the transparency of glass host. BaO acts as an agent for increases the glass formation region of the matrix as well as to reduce the viscosity of the glass host. A uniform distribution of Yb<sub>2</sub>O<sub>3</sub> doped YAG nano-crystals having particle size of 6-10 nm was obtained for the first time to our knowledge into a 0.25

mol% fluorine co-doped silica optical fiber preform made by the MCVD and solution doping technique, and under suitable thermal treatment.

## 7. Geometrical and optical characterizations of nano-engineering fiber

The refractive index profile of nano-engineering fibers was measured by fiber analyser. Using the transmission microscope (Model: Nikon Eclipse LV 100) connected to a high resolution digital colour camera controlled by imaging software, the cross-sectional views of all the fiber sections are taken along with the values of core-clad dimensions. The cross-sectional view along with refractive index profile of  $\text{Yb}_2\text{O}_3$  doped nano-engineering fibers (NYb-6 and NYb-10) having diameter around 17-20 micron are given in Fig. 36 and Fig. 37, respectively.

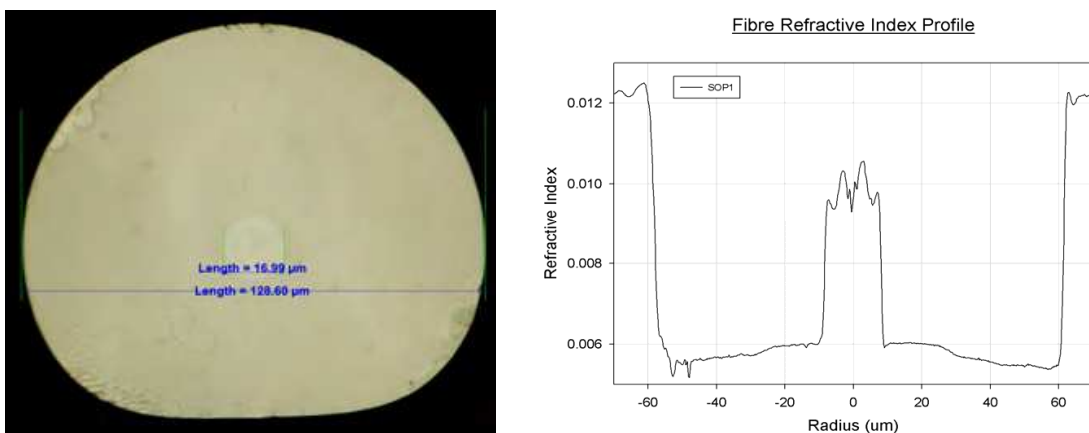


Fig. 36. Cross-sectional view and refractive-index profile of  $\text{Yb}_2\text{O}_3$  doped nano-engineering fiber (NYb-6).

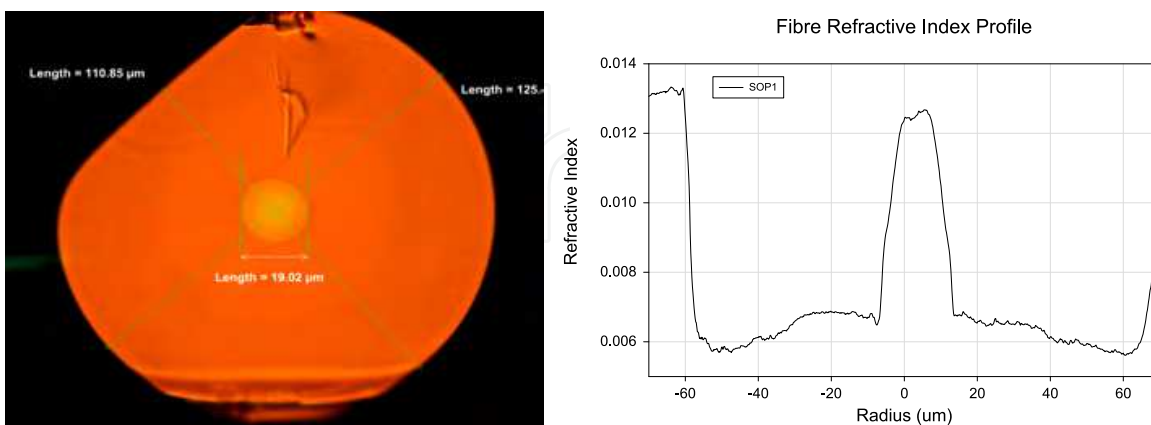


Fig. 37. Cross-sectional view and refractive-index profile of  $\text{Yb}_2\text{O}_3$  doped nano-engineering fiber (NYb-10).

The cross-sectional view of large core nano-engineering fibers (IMNYb-3, IMNYb-12D & IMNYb-12P) having diameter around 25.0 – 35.0 micron along with their refractive index profiles are given in Fig. 38 and Fig. 39 respectively.

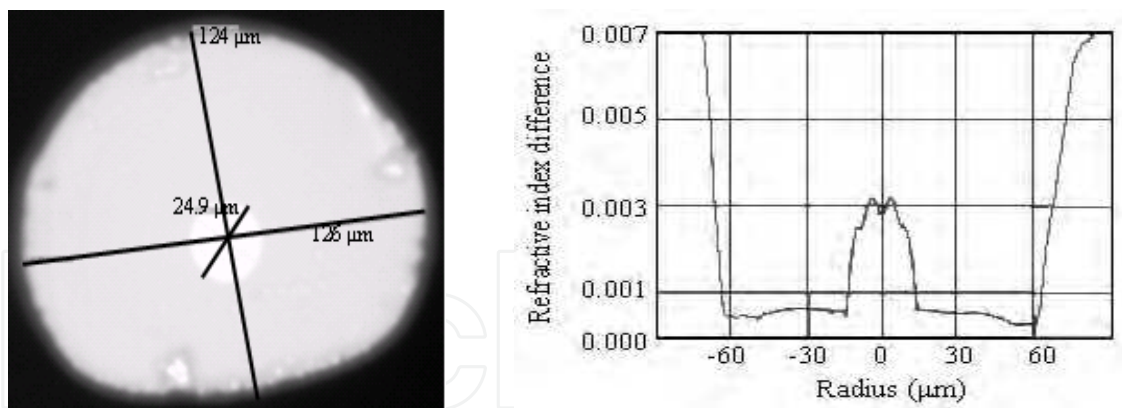


Fig. 38. Cross-sectional view and refractive-index profile of  $\text{Yb}_2\text{O}_3$  doped large core nano-engineering fiber (IMNYb-3) having core diameter around 25.0 micron.

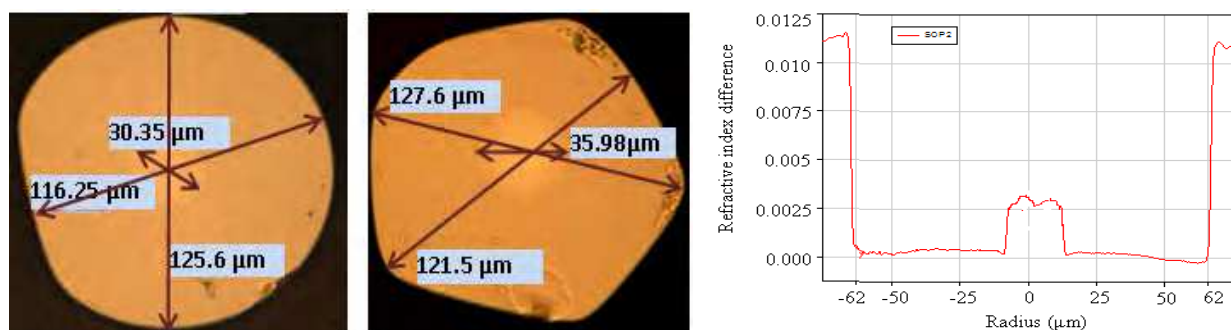


Fig. 39. Cross-sectional view and refractive-index profile of  $\text{Yb}_2\text{O}_3$  doped large core nano-engineering fiber (IMNYb-12D & IMNYb-12P) having core diameter of 30.0 - 35.0 μm.

## 8. Spectroscopic properties of $\text{Yb}_2\text{O}_3$ doped nano-engineering preforms and fibers

The UV-VIS spectra of three preform samples NYb-6, NYb-8 and NYb-9 annealed at  $1450^\circ\text{C}$  was shown in Fig. 40. The instrument used for this purpose was UV-VIS-NIR-3101PC scanning spectrophotometer. The peaks at 220 nm and 380 nm are attributed to the presence of ytterbium oxygen defect center (YbODC) (Yoo et al., 2007) and  $\text{Yb}^{2+}$  ions (Yusong et al., 2007).

The absorbance value of fiber preform NYb-9 becomes much lower than that of NYb-6 and NYb-8. This phenomena indicates that the size of the particles generated within the preform sample NYb-9 becomes lower than that of preforms NYb-6 and NYb-8. The optical absorption spectra of preform NYb-5 annealed at  $1300^\circ\text{C}$  and  $1450^\circ\text{C}$  was shown in Fig. 41. The fiber preform sample NYb-5 annealed at  $1300^\circ\text{C}$  shows two normal absorption peaks centered at 915 and 975nm wavelengths which confirm that Yb ions are present in normal glass matrix. The same preform annealed at  $1450^\circ\text{C}$  had two additional absorption peaks centered at 935 and 960nm which becomes comparable to the absorption peaks centered at 941 and 968 observed in Yb:YAG ceramic samples<sup>41</sup>. Such a small variations in absorption peak positions arise as the crystals are dispersed in silica glass matrix not in a Yb:YAG pure state. Thus optical absorption confirms that YAG crystals are developed within silica glass matrix based fiber preform sample under annealing at  $1450^\circ\text{C}$ .

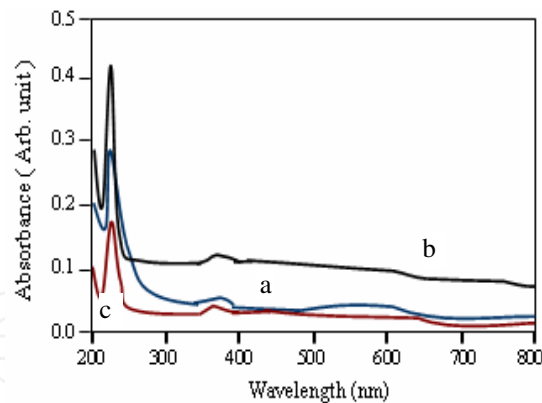


Fig. 40. UV-VIS spectra of three preform samples (a) NYb-6, (b) NYb-8 and (c) NYb-9 annealed at 1450°C.

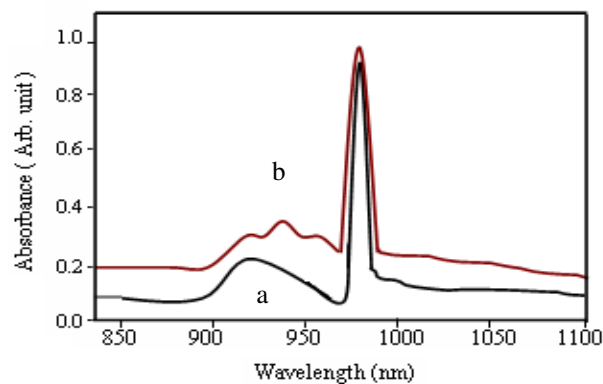


Fig. 41. Optical absorption spectra of preform NYb-5 (a) annealed at 1300°C and (b) 1450°C in NIR region.

The spectroscopic properties of the prepared fibers were investigated and compared to a Yb-doped aluminosilicate (Yb:Al) fiber fabricated in-house. The background loss of the fibers at 1285 nm wavelength was measured by high resolution optical time-domain reflectrometer (OTDR) and presented in Table-1. It was observed that background loss of the fibers very much related to the sizes of the Yb<sub>2</sub>O<sub>3</sub> doped nano-particles. The nano-particles silica fiber NYb-9 having sizes 5-8 nm shows the minimum background loss around 40-50 dB/Km at 1285 nm wavelength. Whereas the nano-particles silica fibers NYb-6, NYb-7 and NYb-8 containing the larger sized particles shows the high background loss. The background loss at 1285 nm was 40-2400 dB/km, depending on the core composition and size of the nano-particles as shown in Table-1. The optical absorption spectra of the fabricated nano-particles fibers NYb-3, NYb-5, NYb-6, NYb-7 and NYb-9 are measured from 350-1750 nm wavelength using white light source and shown in Fig. 42.

The peaks corresponding to 915 and 975 nm are characteristics absorption peaks of Yb<sup>3+</sup> ions (Langnera et al., 2008). The normal fiber NYb-3 and nano-particles fiber NYb-9 shows the minimum absorption loss compared to the fibers NYb-5, NYb-6 and NYb-7 containing larger sized particles. The nano-particle fiber NYb-9 is found to be the best from view point of the formation of very small sized nano-particles within 5-8 nm showing low background loss of 40-50 dB/Km at 1285 nm wavelength.

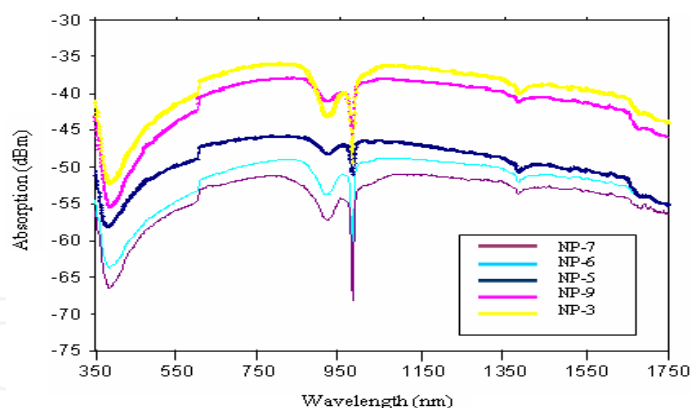


Fig. 42. Optical absorption of different Yb<sub>2</sub>O<sub>3</sub> doped nano-particles silica fibers measured using white light source.

The fluorescence and lifetime of the fibre samples are measured under pumping at 915 and 976 nm wavelengths (Yoo et al., 2010). A fiber-coupled single mode laser diode at 915 nm was used as a pump source. The pump fiber was spliced to a fiber under test and the other end of the test fiber was angle cleaved to suppress any feedback of signal light. Index matching fluid was applied to the output end to further suppress the undesired feedback. The fluorescence was captured by placing one end of a multi-mode fiber to the side of the test fibers. An InGaAs photodetector was connected to the other end of the multi-mode fiber to record fluorescence decay time. The 915 nm laser diode was modulated externally by an acousto-optic modulator in the course of the lifetime measurement. We used less than 5 cm long fibers to avoid amplified spontaneous emission and reabsorption.

Fig. 43 shows the measured decay time with the nanoparticle fiber and the Yb:Al fiber (Yoo et al., 2010). The decay time was determined at the point where the intensity drops to 1/e of its original value. Both decay curves were well fitted with single exponential form. The decay time of the nanoparticle fiber was recorded as ~ 860 μsec which is close to that of Al:Yb fiber. The fitting goodness was better than 0.9996.

Fig. 44 shows measured absorption and fluorescence spectra for the nanoparticle fiber compared to those of Yb:Al fiber. Each peak was scaled to unity to make a spectral shape comparison. We see the spectral shapes of Yb absorption in the nanoparticle fiber are modified against the Yb:Al counterpart, which again indicates the different environments for the Yb ions. However, the line shapes do not follow the Yb-doped Y<sub>2</sub>O<sub>3</sub> ceramic (Bourova et al., 2008) due to the glassy nature of the nanoparticles as confirmed in the TEM analysis (Ballato et al., 2009).

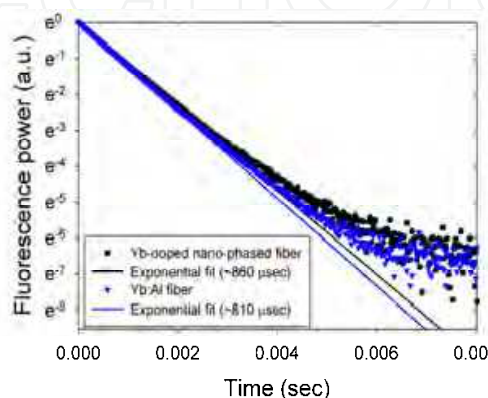


Fig. 43. Fluorescence decay time of Yb-doped nanoparticle silica fiber and Yb:Al fiber.

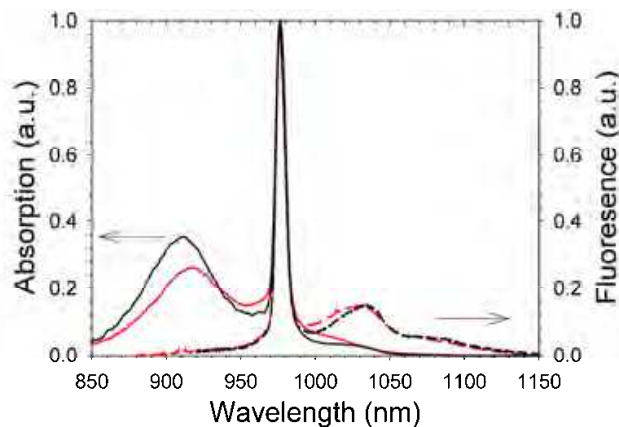


Fig. 44. Spectral shapes of absorption (solid line) and fluorescence (dashed line) of Yb-doped nanoparticle silica fiber (red) and Yb:Al fiber (black).

### 9. Lasing performances of $\text{Yb}_2\text{O}_3$ doped nano-engineering fibers

The Yb-doped nanoparticle fibers were tested under laser configuration (Yoo et al, 2010; Sahu et al, 2009). A D-shaped fiber (NYb-7) in double clad structure was pulled in 400  $\mu\text{m}$  inner cladding diameter. The large inner cladding diameter was chosen to enable an efficient pump launch from the high-power pump diodes. The experimental arrangements are schematically shown in Fig. 45. The fiber was end-pumped by a 975 nm laser diode. Pump launch end of the fiber was cleaved perpendicularly to the fiber axis to provide 4% Fresnel reflection for the laser cavity. At the other end, a high reflective mirror (100%) at signal band was used to close the laser cavity. Most of the launched pump beam was absorbed through the 5 m long fiber. The output power linearly increased with the launched pump power. The output reached 85 W for a launched pump power of 120 W, representing good slope efficiency of 76% with respect to the launched pump power (Sahu et al., 2009) as shown in Fig. 46.

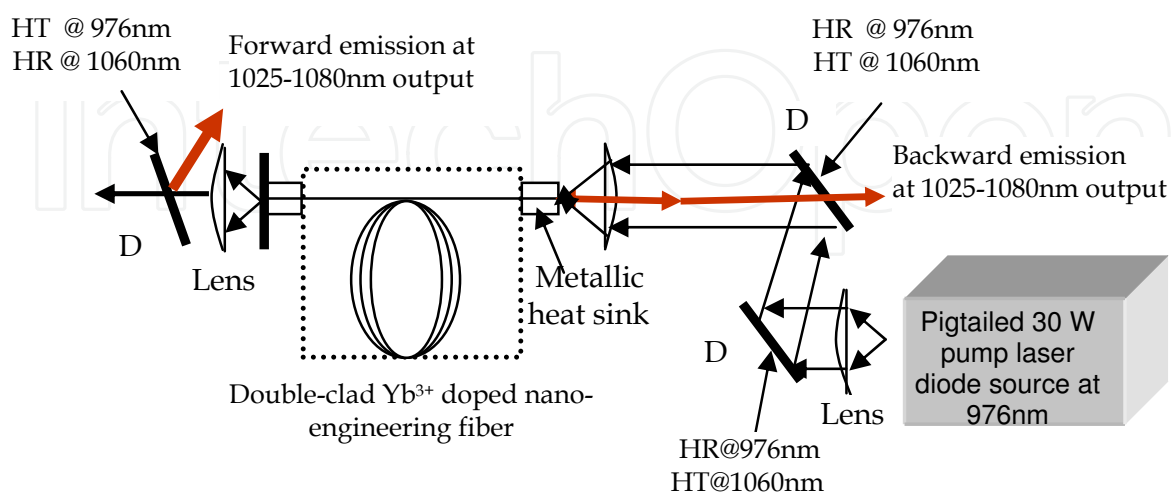


Fig. 45. Experimental arrangement for the laser performance characterization of nano-engineering fibers.

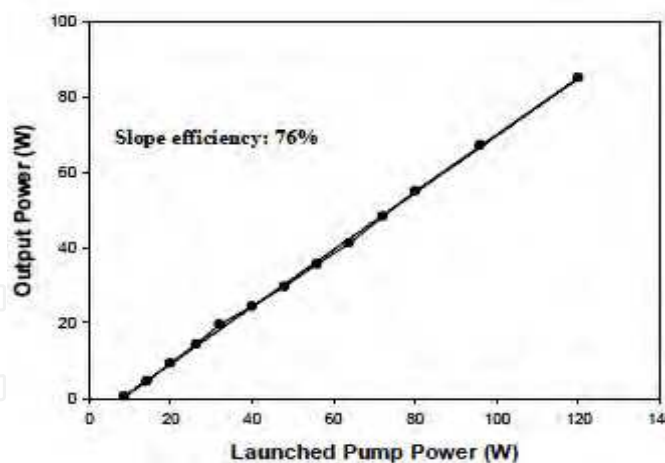


Fig. 46. Laser performance of 4 meter length of nano-engineering fiber (NYb-7).

We further investigated the lasing performance of another nano-engineering fiber (NYb-8) having 125 μm inner cladding diameter along with lasing bands. Fibers with 125 μm inner cladding diameter were placed in a free-running linear 4%-4% laser cavity test bed and the output spectrum was recorded by an OSA. We found that both lasing wavelength and 3dB bandwidth are pump power dependent. Fig. 47(a) represents the pump power dependent of laser spectra in 0.2 nm of OSA resolution. In a 4 m long fiber, the oscillation started at 1057 nm with total 13 dB of pump power absorption. As we increased the pump power, another band appeared at longer wavelength, ~ 1070 nm. The laser operated at two wavelength bands at ~ 1050 and 1070 nm with a gap between.

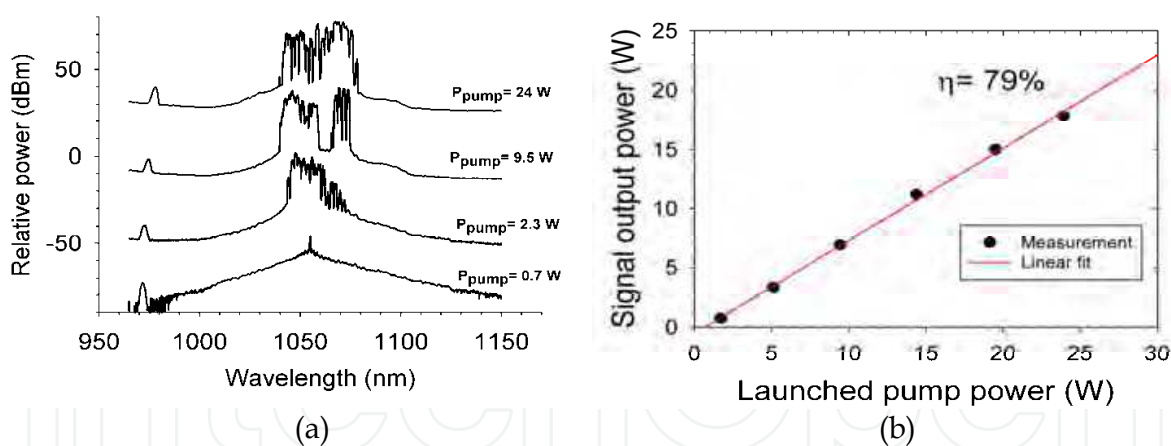


Fig. 47. (a) Pump power dependent lasing band in Yb-doped nanoparticle silica fiber in 4 m length (b) Laser performance of 4 m long Yb-doped nanoparticle silica fiber (NYb-8).

More intense pump power filled the gap and made up a broad band oscillation from 1040-1075 nm. The observed pump power dependent of laser operation band is different as compared to Yb-doped silica fibers in conventional hosts. However, it did not compromise the laser efficiency. The fiber provided laser efficiency of 79% with respect to the launched pump power as shown in Fig. 47 (b). Identification of the cause of this behaviour is under progress.

The lasing characteristic of other nano-particles silica fiber NYb-9 containing fluorine was shown in Fig. 48. The lasing efficiency of such nano-particles silica fiber was observed

around 83.0 % with respect to the absorbed pump power (Paul et al., 2010). The maximum output power was well above 10 W, and limited by available pump power. The fiber containing  $\text{Yb}_2\text{O}_3$  doped yttria rich alumino silica based nano-particles sized within 5-8 nm shows good lasing efficiency around 83.0% with respect to the absorbed pump power compared to the Yb:YAG crystal based ceramic laser (Yusong et al., 2007). The output spectrum of the laser for both forward and backward signal was shown in Fig. 49. Such nano-particles silica fiber shows a broad band oscillation from 1040-1075 nm in their output spectrum.

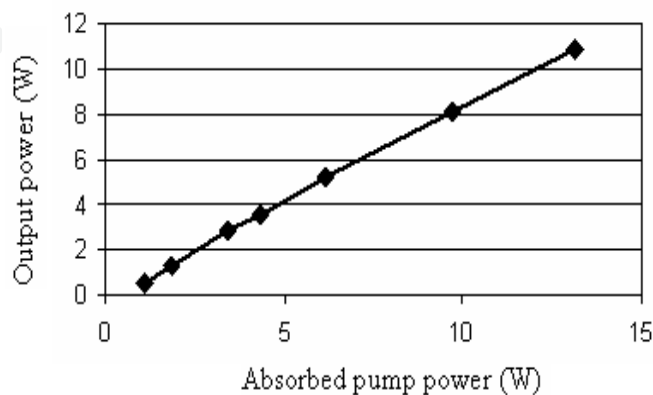


Fig. 48. Laser performance of 4 meter long Yb-doped nano-particle silica fiber NYb-9 under pumping at 975 nm wavelength.

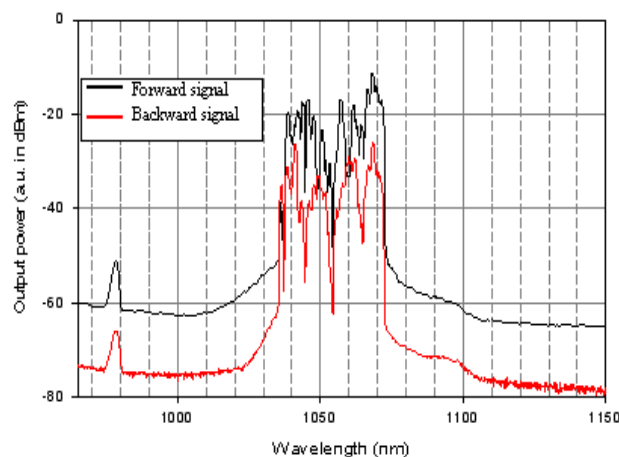


Fig. 49. Output spectrum of the lasing band of forward and backward signal of Yb doped nano particle silica fiber NYb-9 under launched pump power of 16 W by 975 nm pump laser diode.

The lasing characteristics of the fabricated Yb-doped nano-engineering large core fibers (IMNYb-3, IMNYb-12D & IMNYb-12P) pumping at 976 nm by a multi-mode laser diode in the cladding-pump configuration through pump combiner was measured as shown in Fig. 50, Fig. 51 and Fig. 52 respectively. The laser cavity was formed by splicing two fiber Bragg gratings (FBG) with reflectivity 99% (HR) and 10% (LR) at 1080 nm placed at each end of the Yb fiber. The pump wavelength was again 976 nm which provided the excitation within the zero-phonon line of  $\text{Yb}^{3+}$  ion.

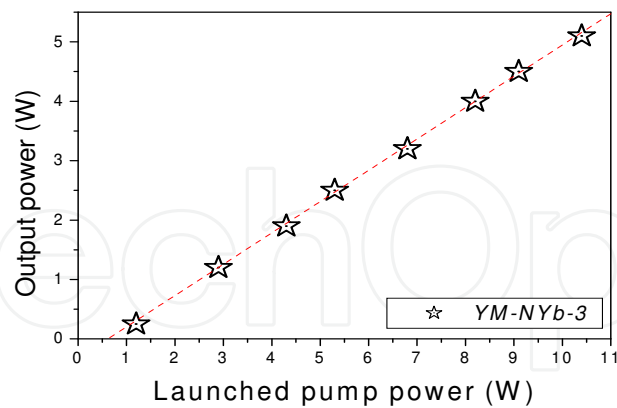


Fig. 50. Laser performance of 4.5 meter long Yb-doped nano-particle silica fiber IMNYb-3 under pumping at 976 nm wavelength.

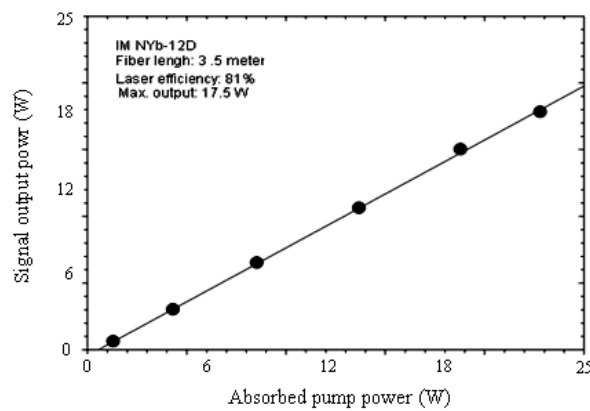


Fig. 51. Laser performance of 3.5 meter long Yb-doped nano-particle silica fiber IMNYb-12D under pumping at 976 nm wavelength.

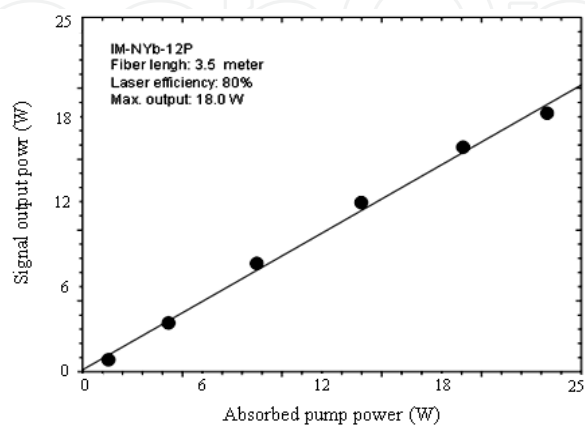


Fig. 52. Laser performance of 3.5 meter long Yb-doped nano-particle silica fiber IMNYb-12P under pumping at 976 nm wavelength.

## 10. Photo-darkening phenomena of nano-engineering fibers

A lot of study was done about PD in silica fibers doped with different RE ions (Broer et al., 1993; Atkins & Carter, 1994; Koponen et al., 2006). PD deteriorates the performance of fiber lasers or amplifiers (Hönninger et al., 2007; Morasse et al., 2007). Such phenomenon is initiated by the high Yb inversion (Koponen et al., 2006; Hönninger et al., 2007). The generation of color centers are responsible for the induced excess loss in the UV/VIS/IR wavelength range and was attributed to a photo-ionization process powered by the energy of excited Yb ions. PD in Yb doped fibers can also be induced by 488 nm irradiation (Yoo et al., 2007). Several measurement techniques to investigate the temporal and spectral characteristics of the loss evolution were developed (Koponen et al., 2006; Hönninger et al., 2007; Morasse et al., 2007; Yoo et al., 2007; Jasapara et al., 2006; Shubin et al., 2006; Koponen et al., 2007). Cladding pumping is advantageous, because a homogeneous Yb inversion can be achieved, independent of the core diameter and adjustable in a wide range with moderate pump powers. The pump induced PD in Yb-doped fibers has been recognized as a bottleneck for power scaling in many applications. It was found that the induced loss is proportional to the inversion level of the Yb<sup>3+</sup> ions. Host material dependence was also reported and phosphosilicate can suppress the PD in a significant amount compared to the aluminosilicate counterpart (Shubin et al., 2007; Jetschke et al., 2008).

Here we have investigated the PD phenomena of Yb doped nanoparticles in a silica rich matrix based optical fibers as an alternative to the Yb in a 'standard', such as aluminium or phosphorous co-doped, silica host for use in high power fiber lasers. It is expected that the Y<sub>2</sub>O<sub>3</sub> nanoparticles within a silica host will modify the Yb environments, which influences host material dependent processes such as PD and rare-earth solubility.

As the spectroscopic properties of the nanoparticle fiber described earlier indicate modification in the surrounding environments of the Yb ions, we expect different behavior of PD in the fibers. The PD was evaluated by monitoring the transmitted probe power at 633 nm through the fiber under test. The PD measurement setup is presented in Fig. 53. We used fiber-coupled single mode 977 nm laser diode as a pump source. The output end of the pump fiber was spliced to one port of wavelength-division multiplexing (WDM) coupler and the pump beam was delivered to the test fiber by splicing the output end of the WDM coupler and the test fiber. A He-Ne laser at 633 nm was used as a probe beam which coupled to the test fiber through the WDM coupler. The probe beam propagated the same direction as the pump beam. The output end of the test fiber was spliced to another WDM coupler to separate the pump and probe beam. The probe beam was chopped by mechanical chopper and the output power was detected by photodiode and lock-in amplifier after passing through the monochromator. We used ~ 1 cm of the test fiber to create uniform universion level of Yb ions and to suppress unwanted amplified spontaneous emission. The pump input power was maintained to provide >35% of population inversion of Yb<sup>3+</sup> throughout the fibers. We carried the PD measurement with the Yb-doped nanoparticle fiber and the Yb:Al fiber. Both fibers were in 125 μm diameter. The small signal absorption in both fibers was around 3 dB/m at 976 nm. The temporal characteristics of the transmitted probe power are represented in Fig. 54. The PD induced loss is significantly reduced in the Yb-doped nanoparticle fiber. When fitted the measured results with stretched exponential form (Shubin et al., 2007), we found that the saturated induced loss in Yb-doped nanocrystalline fiber reduced by 20 times compared to the aluminosilicate counterpart.

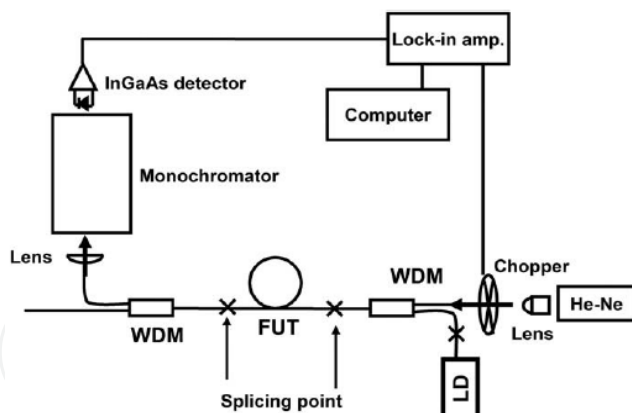


Fig. 53. Photodarkening induced loss measurement setup. FUT: Fiber under test, LD: Laser diode, WLS: White light source.

The PD process is associated with non-binding oxygen near surfaces of ytterbium/aluminium clusters which forms in silica material co-doped with ytterbium and aluminium. The non-binding oxygen originates from  $\text{Yb}^{3+}$  in substitute of  $\text{Si}^{4+}$  sites. When subjecting the ytterbium to 976 nm pump radiation, excess energy is radiated as phonons which cause a lone electron of one non-binding oxygen atom to shift to a nearest neighbour non-binding oxygen atom with creation of a hole and a pair of lone electrons that results in a coulomb field between the oxygen atoms to form an unstable colour centre. The conversion of such unstable colour centre to a semi-stable centre requires the shifting of one electron of the lone electron pair to a nearest neighbour site (Mattsson et al., 2008). In yttria alumino silicate glass matrix the yttrium ( $\text{Y}^{3+}$ ) is chosen as codoping ion since their ionic radius is similar (0.0892 nm for  $\text{Y}^{3+}$  and 0.0985 nm for  $\text{Yb}^{3+}$ ).  $\text{Yb}^{3+}$  and  $\text{Y}^{3+}$  have also the same valence; therefore they can easily substitute its-self and can increase the distance between two  $\text{Yb}^{3+}$  ions. In the case of codoping with  $\text{Yb}^{3+}$  and  $\text{Y}^{3+}$ , the formation of  $\text{Yb-O-Y-O-Yb}$  may be take place just like to the formation of  $\text{Er-O-Y-O-Er}$  as reported by Trinh Ngoc Ha et. al (Ha et al., 2004). As a result of it, the formation of Yb related ODC ( $\text{Yb-Yb}$ ) will be prevented. Hence the phenomenon of PD effect may be reduced.

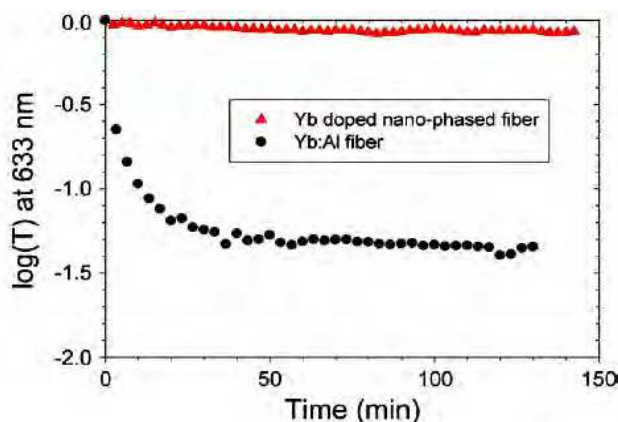


Fig. 54. Temporal characteristics of transmitted power at 633 nm for Yb-doped nanoparticle fiber and Yb:Al fiber.

On the other hand, the UV absorption spectra of  $\text{Yb}_2\text{O}_3$  doped alumino-silicate glass based optical preform and  $\text{Yb}_2\text{O}_3$  doped yttria-alumino silicate glass based optical preform

samples having almost the same doping levels of  $\text{Yb}_2\text{O}_3$  (0.13 mol%) and  $\text{Al}_2\text{O}_3$  (0.9 mol%) was shown in Fig. 55.

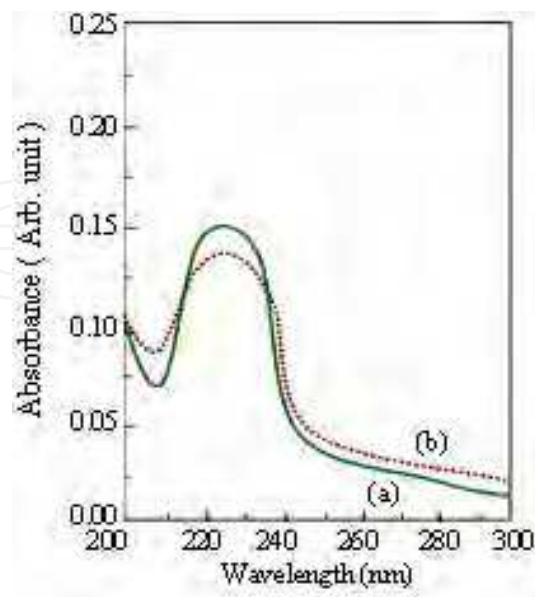


Fig. 55. Absorption spectra of (a)  $\text{Yb}_2\text{O}_3$  doped alumino silicate preform and (b)  $\text{Yb}_2\text{O}_3$  doped yttria alumino silicate preform (NYb-7).

In  $\text{Yb}_2\text{O}_3$  doped alumino silicate glass the peak related to 220-225 nm is associated with the formation of YbODC (Yoo et al., 2007). The peak intensity related to YbODC becomes lower in yttria alumino silicate glass based optical preform compared to alumino-silicate glass based optical preform. This phenomena signifies that the presence of yttria reduces the formation of ytterbium related oxygen defect centers. The PD in the Yb-doped aluminosilicate preform takes place through the breaking of ODCs under two-photon absorption which gives rise to release of free electrons. The released electrons may be trapped at Al or Yb sites and form a color center resulting in PD. The choice of Al and Y as codopants is of due to the same valence of  $\text{Al}^{3+}$ ,  $\text{Y}^{3+}$ , and  $\text{Yb}^{3+}$  as well as similar lattice structure of  $\text{Al}_2\text{O}_3$ ,  $\text{Y}_2\text{O}_3$  and  $\text{Yb}_2\text{O}_3$ . As the field strength of the modifier cation increases, either through decreasing ionic radius or increased charge, it is expected to begin to perturb the aluminosilicate network more strongly, because of the energetic stabilization provided by closer association of negatively charged species, in particular non-bridging oxygen (NBO). In yttria-alumino silicate glass with increasing Y/Si ratio, the  $^{29}\text{Si}$  peak shifts to a higher frequency, indicating a smaller shielding of the Si nucleus because of the substitution of Al by Y, which may be related to the conversion of bridging oxygen (BO) to non-bridging oxygen (NBO) (Schaller & Stebbins, 1998).  $^{27}\text{Al}$  MAS NMR study (Kohli et al., 1992) also demonstrate that one major effect of  $\text{Y}^{3+}$  is to promote the conversion of  $\text{AlO}_4$  groups to higher-coordinate species which provides more oxygen surrounding spaces, thus reducing the number of ODCs, the hypothesized precursor to PD.

## 11. Conclusions

A detail review was done about the development of large core nano-engineered  $\text{Yb}_2\text{O}_3$  doped fiber having diameter around 20-35 micron drawn from nano-crystalline YAG based

silica glass preforms made by MCVD and solution doping technique followed by suitable thermal annealing conditions of the preform. Such nano-particles are developed during drawing of optical fiber from the modified preform which annealed at 1450-1500°C for 3 hours under heating and cooling rates of 20°C/min. The diameter of the doped region was increased from 20 to 35 micron through modification of several fabrication parameters such as number of deposited porous layers, composition of deposited porous layers and CSA of the starting deposited tube. The uniform doping levels within the large core fiber preforms was maintained through optimization of the deposition temperature with respect to composition and numbers of the deposited porous layers as well as thickness of the silica tube with varying inner diameter of the tube prior to deposition. The effect of phosphorous and fluorine doping on nano-structuration of  $\text{Yb}_2\text{O}_3$  doped fiber was discussed in details. The formation of nano-particles occurs through the phase separation phenomena and crystal growth mechanisms which normally occur in bulk silica-based glass. The size and shape of the nano-particles were evaluated from the TEM results. The crystalline nature of nano-particles was observed after annealing at 1450°C. In presence of P the average nano-crystallites size of 25-50 nm were homogeneously dispersed within the core region. The crystal size increases as the  $\text{P}_2\text{O}_5$  doping level increases due to the strong field strength difference of  $\text{P}^{5+}$  and  $\text{Si}^{4+}$  ( $>0.3$ ) where  $\text{P}_2\text{O}_5$  serves as a nucleating agent to accelerate the growth of formation of large crystallites. A bimodal size distribution with larger particles of the order of 60 nm and the smaller ones of 3-5 nm in diameter was observed in presence of P where most likely P and F together play a different kind of nucleation and crystallization phenomenon for such kind of bimodal distribution. By adding fluorine to the silica based composition, nano particles of 6-10 nm in diameter are obtained. The composition of phase-separated crystalline particles was evaluated by comparing their EDX data, taken directly from the crystal particles and from an area outside of the particles. The EDX spectra taken from the crystal particles detected Si, Al, O, Yb and Y signals, whereas the areas outside of the particles detected Si, Al and O and no Yb and Y. The compositional analyses of the phase-separated nano-particles consists of 13.0 atom % of Al, 0.02 atom% of Yb, 9.0 atom % of Y and 36.0 atom% of O. The doping level of the formation of Yb:YAG crystals (confirmed from the XRD spectra) within fiber preform sample is found to be 0.02 atom%. The phase-separated crystalline nano-particles were developed within the central core glass matrix under post-heat treatment within 1450-1500°C for a period of 3 hours. Such annealed preform shows two additional absorption peaks centered at 935 and 960 nm indicating the formation of Yb:YAG crystals. The main feature of such process involves the direct synthesis of Yb:YAG nano-crystallites within the core of optical fiber preform through the conventional MCVD and solution doping technique. However nature of the particles was changed from crystalline to amorphous at fiber drawing stage when fiber drawn from such annealed preform after heating at 2000°C within fiber drawing furnace. The TEM spectra reveal the size of the particles within 6-10 nm. The energy dispersive X-ray (EDX) spectra signifies that yttrium and ytterbium are dominant in phase-separated particles whilst they are sparse in the non-phase-separated region. The background loss of such nano-particles based fibers is maintained within 40-50 dB/Km by keeping the particle sizes within 6-10 nm range. The fiber containing 6-10 nm sizes of  $\text{Yb}_2\text{O}_3$  doped yttria alumino rich silica based nano-particles shows good lasing efficiency around 80% with respect to the absorbed pump power compared to the Yb:YAG crystal based ceramic laser. Such nano-engineering fiber shows a broad band lasing oscillation from 1040-1075 nm.

More generally, this concept has great potentials as possible solutions to now a days issues in lasing fibers specifically PD phenomenon under high power application as well as fiber amplifiers for intrinsic gain flattening and spectral hole burning.

## 12. Future direction

The future work involves the fabrication of optical fiber based on suitable host of advanced nano-engineered rare-earth doped modified silica glass of 85-90% SiO<sub>2</sub> containing heavy metals and semi-conductors through solution doping process followed by MCVD technique. The aspect of such kind of future work will reveal the suppression of PD phenomena to stabilize the lasing output power through modification of the surrounding environments of RE ions which embedded into different nano-engineering hosts. The future work will also focus the making of large core area upto 35.0 μm diameter nano-engineering optical fibers with uniform distribution of phase-separated nano-particles from view point of good lasing efficiency at high power applications.

Extended X-ray absorption fine structure (EXAFS) analyses will be carried out for determination of the structural details of the site occupied by the Yb<sup>3+</sup> ion into such nano-engineered glass. X-ray Absorption Spectroscopy at the Yb-L<sub>III</sub> edge (E=8944 eV) and X-ray Powder Diffraction measurements will be done at the GILDA-CRG beamline at the European Synchrotron Radiation Facility (ESRF), France.

Although nano-material doping technology has opened a new way in developing novel special optical fiber, however, as far as we know, there are few work about optical fiber amplification based on silica fiber doped with nano-semiconductor materials. In future work, we will demonstrate a novel special silica fiber doped with InP and ZnS semiconductor nano-particles into the core. Due to the nano size, semiconductor nano-particles will show remarkable quantum confinement effect and size tunable effect, which may provide excellent amplification features. Such nanostructuring of doped fiber will be proposed as a new route to 'engineer' the local dopant environment. All these results will benefit to optical fiber components such as lasers, amplifiers and sensors, which can now be realized with silica glass.

## 13. Acknowledgements

The authors wish to acknowledge CSIR and the Royal Society, UK for provision of financial support under CSIR-Royal Society Joint Collaborative Research Work (2007/R2). The authors also wish to acknowledge DST (Government of India) and CONACYT (Government of Mexico) for providing financial support through the Program of cooperation in science and technology between India and Mexico. The authors would like to thank to the Electron Microprobe Laboratory (University of Minnesota, USA) for performing the EPMA. The authors (1 and 3) are thankful to Prof. Indranil Manna, Director, CGCRI for his continuous encouragement, guidance and support in this work.

## 14. References

- Atkins, G. R. & Carter, A. L. G. (1994). Photodarkening in Tb<sup>3+</sup>-doped phosphosilicate and germanosilicate optical fibers. *Optics Letter*, Vol. 19, No. 12, pp. 874-876, ISSN 0146-9592.

- Ballato, J., Hawkins, T., Foy, P., Kokuoz, B., Stolen, R., McMillen, C., Daw, M., Su, Z., Tritt, T. M., Dubinskii, M., Zhang, J., Sanamyan, T. & Matthewson, M. J. (2009). On the fabrication of all-glass optical fibers from crystals. *Journal of Applied Physics*, Vol. 105, No. 5, pp. 053110-053118, ISSN 0021-8979.
- Bandyopadhyay, T., Sen, R., Dasgupta, K., Bhadra, S. K. & Paul, M. C. (2004). Process for making rare earth doped optical fiber. *US patent 6751990*.
- Bhadra, S. K., Sen, R., Pal, M., Paul, M. C. Naskar, M. K., Chatterjee, S., Chatterjee, M. & Dasgupta, K. (2003). Development of rare-earth doped fibres for amplifiers in WDM system. *IEE Proceedings of Circuits, Devices & Systems*, Vol. 150, No. 6, pp. 480-485, ISSN 1350-2409.
- Blanc, W., Dussardier, B. & Paul, M. C. (2009). Er-doped oxide nanoparticles in silica-based optical-fibers. *GlassTechnology: European Journal of Glass Science and Technology*, Vol. A50, pp. 79-81, ISSN 0017-1050.
- Bourova, E., Billancourt, B., Blanchandin, S., Leplingard, F. & Lasas, J. (April 8, 2008). Active optical fiber for Raman amplification. *US patent 7355788B2*.
- Broer, M. M., Krol, D. M. & DiGiovanni, D. J., (1993). Highly nonlinear near-resonant photodarkening in a thulium-doped aluminosilicate glass fiber. *Optics Letter*, Vol. 18, No. 10, pp. 799-801, ISSN 0146-9592.
- Chryssou, C. E., Kenyon, A. J., Iwayama, T. S., Pitt, C. W. & Hole, D. E. (1999). *Journal of Applied Physics Letter*, Vol. 75, No. 14, pp. 2011-2013, ISSN 0003-6951.
- Cho, J. S., Paek, U. C., Han, W. T. & Heo, J. (2001). Fabrication and heat treatment effects on absorption characteristics of glass fibers doped with PbTe semiconductor quantum dots. *Optical Fiber Communication Conference, OSA Technical Digest Series*, Optical Society of America, ISSN 1-55752-655-9, California, March 2001.
- Chou, J. S. & Lee, S. C. (1994). The initial growth mechanism of silicon oxide by liquid phase deposition. *Journal of Electrochemical Society*, Vol. 141, pp. 3214-3218, ISSN 0013-4651.
- Chen, J. C. (2006). Spectroscopic study on the fluorescence of Cr ions in double-clad Cr:YAG crystal fiber. *Ph. D Thesis*, Institute of Electro-Optical Engineering, National Sun Yat-Sen University, Taiwan.
- Dove, J. F., Russell, H., Kim, J.-S., Nivartvong, N., Flattery, J., Keller, D., & Kornreich, P. G. (2001). Light amplification by a Cd<sub>3</sub>P<sub>2</sub> cylinder fiber. *Proceeding of SPIE*, No. 4216, pp. 62-66, ISBN 9780819438812, February 2001.
- De, G., Qin, W., Zhang, J., Wang, Y., Cao, C. & Cui, Y. (2006). Upconversion luminescence properties of Y<sub>2</sub>O<sub>3</sub>:Yb<sup>3+</sup>,Er<sup>3+</sup> nanostructures. *Journal of Luminescence*, Vol. 119, pp. 258-263, ISSN 0022-2313.
- Fujii, M., Yoshida, M., Hayashi, S. & Yamamoto, K. (1998). Photoluminescence from SiO<sub>2</sub> films containing Si nanocrystals and Er: Effects of nanocrystalline size on the photoluminescence efficiency of Er<sup>3+</sup>. *Journal Applied Physics*. Vol. 84, pp. 4525-4531, ISSN 0021-8979.
- Gonçalves, M. C., Santos, L. F. & Almeida, R. M. (2002). Rare-earth-doped transparent glass Ceramics. *Comptes Rendus Chimie*, Vol. 5, pp. 845-854, ISSN 1631-0748.
- Ha, T. N., Thang, P. N., Chung, L. N., Nga, P. T., Hoi, P. V., Luat, L.V., Cham, T. T., Lien, V. T. K., Barthou L. C. & Benalloul, P. (2004). *International Workshop on Photonics and Applications*. Hanoi, Vietnam, April 2004.

- Hageman, V. B. M. & Oonk, H. A. J. (1986). Liquid Immiscibility in the  $\text{SiO}_2\text{-MgO}$ ,  $\text{SiO}_2\text{-SrO}$ ,  $\text{SiO}_2\text{-La}_2\text{O}_3$ , and  $\text{SiO}_2\text{-Y}_2\text{O}_3$  Systems. *Journal of Physics Chemistry of Glasses*, Vol. 27, No. 5, pp. 194-198, ISSN 0031-9090.
- Hudon, H. & Baker, D. R. (2002). The Nature of Phase Separation in Binary Oxide Melts and Glasses: I. Silicate Systems. *Journal of Non-Crystalline Solids*, Vol. 303, pp. 299-345, ISSN 0022-3093.
- Homma, T., Katoh, T., Yamada, Y. & Murao, Y. (1993). A Selective  $\text{SiO}_2$  Film-Formation Technology Using Liquid-Phase Deposition for Fully Planarized Multilevel Interconnections. *Journal of the Electrochemical Society*, Vol. 140, No. 8, pp. 2410-2414, ISSN 0013-4651.
- Hammersley, A. P., Svensson, S. O., Hanfland, M., Fitch, A. N. & Häusermann, D. (1996). Two-dimensional detector software: From real detector to idealised image or two-theta scan. *High Pressure Research*, Vol. 14, No. 4, pp. 235-248, ISSN 0895-7959.
- Hönninger, I. M., Boulet, J., Cardinal, T., Guillen, F., Podgorski, M., Doua, R. B. & Salin, F. (2007). Photodarkening and photobleaching of an ytterbium-doped silica double-clad LMA fiber. *Optics Express*, Vol. 15, No. 4, pp. 1606-1611, ISBN 1094-4087.
- Izawa, T. & Sudo, S. (1987). *Optical Fibers: Materials and Fabrication*, KTK Scientific Publishers, ISBN 9027723788, Tokyo.
- Jander, P. & Brocklesby, W. S. (2004). Spectroscopy of yttria-alumina-silica glass doped with thulium and erbium. *IEEE Journal of Quantum Electron*, Vol. 40, No. 5, pp. 509-512, ISSN 0018-9197.
- Jasapara, J., Andrejco, M., DiGiovanni, D. & Windeler, R. (2006). Effect of heat and  $\text{H}_2$  gas on the photodarkening of  $\text{Yb}^{3+}$  fibers. *Proceeding of Lasers and Electro-Optics/Quantum Electronics and Laser Science Conference and Photonic Applications Systems Technologies, Technical Digest*, ISBN 978-1-55752-813-1, Optical Society of America, Washington, DC, May 2006.
- Jetschke, S., Unger, S., Schwuchow, A., Leich, M. & Kirchhof, J. (2008). Efficient Yb laser fibers with low photodarkening by optimization of the core composition, *Optics Express*, Vol. 16, No. 20, pp. 15540-15545, ISSN 1094-4087.
- Jiang, X., Song, Q., Xu, L., Fu, J. & Tong, L. (2007). Microfiber knot dye laser based on the evanescent-wave-coupled gain. *Journal of Applied Physics Letters*, Vol. 90, No. 23, pp. 233501-233503 (2007), ISSN 0003-6951.
- John, J. S., Coffey, J. L., Chen, Y. D. & Pinizzotto, R. F. (1999). Synthesis and characterization of discrete luminescent erbium-doped silicon nanocrystals. *Journal of American Chemical Society*. Vol. 121, No. 9, pp. 1888-1892, ISSN 0002-7863.
- Joint Committee on Powder Diffraction Standards, data file. 38-0222.
- Kawanishi, S., Ohmori, M., Tanaka, M. & Sakaki, H. (2006). Observation of photoluminescence of semiconductor nanocrystal quantum dots in the core of photonic band gap fiber. *Tech. Digest of IEEE LEOS meeting*, ISBN 978-1-55752-856-8, San Diego, CA February 2008.
- Klopp, P., Griebner, U., Petrov, V., Griebner, U., Petermann, K., Peters, V. & Ebert, G. (2004). Highly efficient mode locked Yb:Sc<sub>2</sub>O<sub>3</sub> laser. *Optics Letter*, Vol. 29, No. 4, pp. 391-393, ISSN 0146-9592.
- Kohli, J. T., Shelby, J. E. & Frye, J. S. (1992). A structural investigation of yttrium aluminosilicate glasses using Si-29 and Al-27 magic-angle spinning nuclear

- magnetic resonance *Journal Physics Chemistry of Glasses*, Vol. 33, pp. 73-78, ISSN 0031-9090.
- Koponen, J. J., Söderlund, M. J. & Hoffman, H. J. (2006). Measuring photodarkening from single-mode ytterbium doped silica fibers. *Optics Express*, Vol. 14, pp. 11539-11544, ISSN 1094-4087.
- Koponen, J., Söderlund, M., Hoffman, H. J., Kliner, D. & Koplrow, J. (2007). Photodarkening Measurements in Large-Mode-Area Fibers. *Proceedings of the SPIE 6453*, ISBN 9780819465665, March 2007.
- Langnera, A., Schotza, G., Suchb, M., Kayserb, T., Reichelc, V., Grimm, S., Kirchhofc, J., Kraused, V. & Rehmannd, G. (2008). A new material for high-power laser fibers. *Proceedings of the SPIE*, 6873, ISBN 9780819470485, April 2008.
- Lu, J., Lv, J., Murai, T., Takaichi, T., Uematsu, T., Ueda, K., Yagi, H., Yanagitani, T. & Kaminskii, A. (2001). Nd<sup>3+</sup>:Y<sub>2</sub>O<sub>3</sub> ceramic laser. *Japanese Journal of Applied Physics*, Vol. 40, L1277-1279, ISSN 0021-4922.
- Li, T. (1985). *Optical Fiber Communications*, Academic press, ISBN 0 12 447301 6, New York.
- Lu, Q., Li, A., Guo, F. U., Sun L. & Zhao, L. C. (2008). The two-photon excitation of SiO<sub>2</sub>-coated Y<sub>2</sub>O<sub>3</sub>:Eu<sup>3+</sup> nanoparticles by a near-infrared femtosecond laser. *Nanotechnology*, Vol. 19, No. 20, pp. 205704-205711, ISSN 1687-9503.
- Lu, Q., Li, A., Guo, F. U., Sun L. & Zhao, L. C. (2008). Experimental study on the surface modification of Y<sub>2</sub>O<sub>3</sub>:Tm<sup>3+</sup>/Yb<sup>3+</sup> nanoparticles to enhance upconversion fluorescence and weaken aggregation. *Nanotechnology*, Vol. 19, No. 14, pp. 145701-205709, ISSN 1687-9503.
- Mattsson, K. E., Knudsen, S. N., Cadier, B. & Robin, T. (2008). Photo darkening in ytterbium co-doped silica material. *Proceedings of the SPIE*, 6873, ISBN 9780819470485, May 2008.
- Miller, S. E. & Chynoweth, A. G. (1979). *Optical Fiber Telecommunications*, Academic Press, ISBN 0124973507, 9780124973503, New York.
- Morasse, B., Chatigny, S., Gagnon, E., Hovington, C., Martin, J. P. & De Sandro, J. P. (2007). Low photodarkening single cladding ytterbium fibre amplifier. in *Fiber Lasers IV: Technology, Systems, and Applications*, D. J. Harter, A. Tünnermann, J. Broeng, and C. Headley, eds., *Proceedings of the SPIE 6453*, 64530H-1-9.
- Morimoto, S. (2004). Optical Absorption of Cr-containing Li<sub>2</sub>O-SiO<sub>2</sub> system transparent glass-ceramics. *Journal of the Ceramic Society of Japan*, Vol. 112, pp. 130-132, ISSN 1882-0743.
- Morimoto, S., & Emem, W. (2005). Strength of Li<sub>2</sub>O-SiO<sub>2</sub> System Transparent Glass-Ceramics. *Journal of the Ceramic Society of Japan*, 112, 259-262, ISSN 1882-0743.
- Mun, J. H., Novoselov, A., Yoshikawa, A., Boulon, G. & Fukuda, T. (2005). Growth of Yb<sup>3+</sup>-doped Y<sub>2</sub>O<sub>3</sub> single crystal rods by the micro-pulling-down method. *Materials Research Bulletin*, Vol. 40, No. 8, pp. 1235-1243, ISSN 0025-5408.
- Nichols, W.T., Keto, J.W., Henneke, D. E., Brock, J., Malyavanatham, R. G. & Becker, M. F. (2001). Large-scale production of nanocrystals by laser ablation of microparticles in a flowing aerosol *Journal of Applied Physics Letter*, Vol. 78, pp. 1128-1130, ISSN 0003-6951.
- Patra, A., Saha, S., Alencar, M. A. R. C., Rakov, N. & Maciel, G. S. (2005). Blue upconversion emission of Tm<sup>3+</sup>- Yb<sup>3+</sup> in ZrO<sub>2</sub> nanocrystals: Role of Yb<sup>3+</sup> ions. *Chemical Physics Letters*, Vol. 407, No. 4-6, pp. 477-481, ISSN 0009-2614.

- Paul, M. C., Bysakh, S., Das, S., Bhadra, S. K., Pal, M., Yoo, S., Kalita, M. P., Boyland, A. & Sahu, J. K. (2010). Yb<sub>2</sub>O<sub>3</sub>-doped YAG nano-crystallites in silica-based core glass matrix of optical fiber preform. *Materials Science and Engineering B*, Vol. 175, No. 2, pp. 108-119, ISSN 0921-5107.
- Paul, M. C., Upadhyaya, B. N., Das, S., Dhar, A., Pal, M., Kher, S., Dasgupta, K., Bhadra, S. K. & Sen, R. (2010). Study of the fabrication parameters of large core Yb<sub>2</sub>O<sub>3</sub> doped optical fibre through solution doping technique. *Optics Communications*, Vol. 283, pp. 1039-1046, ISBN 0030-4018.
- Petermann, K., Fornasiero, L., Mix, E. & Peters, V. (2002). High melting sesquioxides: crystal growth, spectroscopy and laser experiments. *Optical Materials*, Vol. 19, pp. 67-71, ISSN 0925-3467.
- Rajala, M., Janka, K. & Kykkänen, P. (2003). An industrial method for nanoparticle synthesis with a wide range of compositions. *Review on Advanced Materials Science*, Vol. 5, pp. 493-497, ISSN 1605-8127.
- Rawson, H. (1967). *Inorganic Glass-Forming Systems*, Academic Press, ISBN 012583750X, London.
- Ray, N. H. (1974). Composition-property relationships in inorganic oxide glasses. *Non-Crystalline Solids*, Vol. 15, pp. 423, ISSN 0022-3093.
- Sahu, J. K., Paul, M. C., Kalita, M. P., Boyland, A., Codemard, C., Yoo, S., Webb, A., Standish, R. J., Nilsson, J., Das, S., Bhadra, S. K., Pal, M., Dhar, A. & Sen, R. (2009). Ytterbium doped nanostructured optical fibers for high power fiber lasers. *Conference on Lasers and Electro-Optics, CLEO-2009*, Baltimore, MD, ISBN 978-1-55752-869-8.
- Samson, B.N., Pinckney, L. R., Wang, J., Beall, G. H. & Borrelli, N. F. (2002). Nickel-doped nanocrystalline glass- ceramic fiber. *Optics Letters*, Vol. 27, No. 15, pp. 1309-1311, ISSN 0146-9592.
- Samson, B. N., Tick, P. A. & Borrelli, N. F. (2001). Efficient neodymium-doped glass-ceramic fiber laser and amplifier. *Optics Letters*, Vol. 26, No. 3, pp. 145-147, ISSN 0146-9592.
- Schaller, T. & Stebbins, J. F. (1998). The structural role of lanthanum and yttrium in aluminosilicate glasses: A <sup>27</sup>Al and <sup>17</sup>O MAS NMR study. *Journal of Physical Chemistry B*, Vol. 102, No. 52, pp. 10690-10697, ISSN 1089-5647.
- Sen, R., Pal, M., Paul, M. C., Bhadra, S. K., Chatterjee, S. & Dasgupta, K. (2005). *Method of fabricating rare earth doped optical fiber*. US patent 6851281.
- Shannon, R.D. (1976). *Revised effective ionic radii and systematic studies of interatomic distances in halides and chalcogenides*. *Acta Crystallographica Section A*, Vol. 32, No. 5, pp. 751-767, ISSN 0108-7673.
- Shelby, J. E. (1997). *Introduction to glass science and technology*, Royal Society of Chemistry, ISBN 0854045333, UK.
- Shi, L., Xu, Y., Tan, W. & Chen, X. (2007). Simulation of optical microfiber loop resonators for ambient refractive index sensing. *Sensors* Vol. 7, No. 5, pp. 689-696, ISSN 1424-8220.
- Shirakawa, A., Takaichi, K., Yagi, H., Tanisho, M., Bisson, J.-F., Lu, J., Ueda, K., Yanagitani T. & Kaminskii, A. A. (2004). First mode-locked ceramic laser: Femtosecond Yb<sub>3+</sub>:Y<sub>2</sub>O<sub>3</sub> ceramic laser, *Journal of Laser Physics*, Vol. 14, pp. 1375-1381, ISSN 1054-660X.

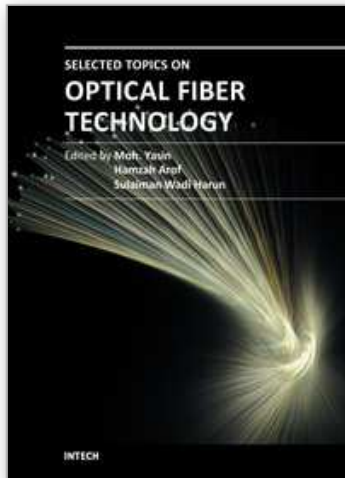
- Shirakawa, A., Takaichi, K., Yagi, H., Bisson, J. F., Lu, J., Musha, M., Ueda, K., Yanagitani, T., Petrov, T. S. & Kaminskii, A. A. (2003). Diode-pumped mode-locked Yb<sup>3+</sup>:Y<sub>2</sub>O<sub>3</sub> ceramic laser. *Optics Express*, Vol. 11, No. 22, pp. 2911-2916, ISSN 1094-4087.
- Shirakawa, A., Takaichi, K., Yagi, H., Bisson, J., Lu, J., Musha, M., Ueda, K., Yanagitani, T., Petrov, T. & Kaminskii, A. (2003). Diode-pumped mode-locked Yb<sup>3+</sup>:Y<sub>2</sub>O<sub>3</sub> ceramic laser. *Optics Express*, Vol. 11, No. 22, pp. 2911-2916, ISSN 1094-4087.
- Shubin, A. V., Yashkov, M. V., Melkumov, M. A., Smirnow, S. A., Bufetov, I. A. & Dianov, E. M. (2007). Photodarkening of aluminosilicate and phosphosilicate Yb-doped fibers. *Lasers and Electro-Optics 2007 and International Quantum Electronics Conference, CLEOE-IQEC 2007*, ISBN 978-1-4244-0931-0, June 2007.
- Tomozawa, M., Doremus, R. H., Tomozawa, M. & Doremus, R. H. (1978) *Glass I: Interaction with Electromagnetic Radiation*, ISBN Academic, New York, Vol. 12, pp. 5-89
- Takaichi, K., Yagi, H., Lu, J., Bisson, J. F., Shirakawa, A., Ueda, K., Yanagitani, K. & Kaminskii, A. A. (2004). Highly efficient continuous-wave operation at 1030 and 1075 nm wavelengths of LD pumped Yb<sup>3+</sup> : Yb<sub>2</sub>O<sub>3</sub> ceramic lasers. *Applied Physics Letter*, Vol. 84, pp. 317-319, ISSN 0003-6951.
- Tomazawa, M. & Doremus, R. H. (1979). *Treatise on Materials Science and Technology*, Academic Press, New York.
- Townsend, J. E., Poole, S. B. & Payne, D. N. (1987). Solution doping technique for fabrication of rare earth doped optical fibers. *Electronics Letter*, Vol. 23, pp. 329-331, ISSN 0013-5194.
- Ubal dini, A. & Carnasciali, M. (2008). Raman characterisation of powder of cubic RE<sub>2</sub>O<sub>3</sub> (RE = Nd, Gd, Dy, Tm, and Lu), Sc<sub>2</sub>O<sub>3</sub> and Y<sub>2</sub>O<sub>3</sub>. *Journal of Alloys Compounds*, Vol. 454, No. 1-2, pp. 374-378, ISSN 0925-8388.
- Varshneya, A. K. (1994). *Fundamentals of inorganic glasses*, Academic Press. ISBN 978-0-12-714970-7, San Diego, CA.
- Vetrone, F., Boyer, J. C., Capobianco, J. A., Speghini, A. & Bettinelli, M. (2003). Effect of Yb<sup>3+</sup> codoping on the upconversion emission in nanocrystalline Y<sub>2</sub>O<sub>3</sub>:Er<sup>3+</sup>. *Journal of Physical Chemistry B*. Vol. 107, No. 5, pp. 1107-1112, 1089-5647.
- Vogel, W. (1994). *Glass Chemistry*, ISBN 3-540-57572-3, Springer-Verlag, Berlin.
- Yeatman, E. M., Ahmad, M. M., McCarthy, O., Martucci, A., & Guglielmi, M. (2000). Sol-gel fabrication of rare-earth doped photonic components. *Journal of sol-gel science technology*, Vol.19, pp. 231-236, ISSN 0928-0707.
- Yoo, S., Paek, U. C. & Han, W.T. (2003). (2003). Development of a glass optical fiber containing ZnO-Al<sub>2</sub>O<sub>3</sub>-SiO<sub>2</sub> glass-ceramics doped with Co<sup>2+</sup> and its optical absorption characteristics. *Journal of Non-Crystalline Solids*. Vol. 315, No. 1-2, pp. 180-186, ISSN 0022-3093.
- Yoo, S., Basu, C., Boyland, A. J., Sones, C., Nilsson, J., Sahu, J. K., Payne, D. (2007). Photodarkening in Yb-doped aluminosilicate fibers induced by 488 nm irradiation. *Optics Letter*, Vol. 32, No. 12 pp. 1626-1628, ISSN 0146-9592.
- Yoo, S., Kalita, M. P., Boyland, A. J., Webb, A. S., Standish, R. J., Sahu, J. K., Paul, M. C., Das, S., Bhadra, S. K. & Pal, M. (2010). Ytterbium-doped Y<sub>2</sub>O<sub>3</sub> nanoparticle silica optical fibers for high power fiber lasers with suppressed photodarkening. *Optics Communications* Vol. 283, No. 18, pp. 3423-3427, ISBN 0030-4018.

Yusong, W., Jiang, L., Yubai, P., Jingkun, G., Benxue, J., Yi, X. & Jun, X. (2007). Diode-pumped Yb:YAG ceramic laser. *Journal of American Ceramic Society*, Vol. 90, No. 10, pp. 3334-3337, ISSN 1551-2916.

Zarzycki, J. (1991). *Glasses and the vitreous state (First edition)*, Cambridge University Press, ISBN 0 521 35582 6, Press Syndicate of the University of Cambridge.

IntechOpen

IntechOpen



## **Selected Topics on Optical Fiber Technology**

Edited by Dr Moh. Yasin

ISBN 978-953-51-0091-1

Hard cover, 668 pages

**Publisher** InTech

**Published online** 22, February, 2012

**Published in print edition** February, 2012

This book presents a comprehensive account of the recent advances and research in optical fiber technology. It covers a broad spectrum of topics in special areas of optical fiber technology. The book highlights the development of fiber lasers, optical fiber applications in medical, imaging, spectroscopy and measurement, new optical fibers and sensors. This is an essential reference for researchers working in optical fiber researches and for industrial users who need to be aware of current developments in fiber lasers, sensors and other optical fiber applications.

### **How to reference**

In order to correctly reference this scholarly work, feel free to copy and paste the following:

M. C. Paul, A. V. Kir'yanov, S. Bysakh, S. Das, M. Pal, S. K. Bhadra, M. S. Yoo, A. J. Boyland and J. K. Sahu (2012). Fabrication of Large Core Yb<sub>2</sub>O<sub>3</sub> Doped Phase Separated Yttria-Alumino Silicate Nano-Particles Based Optical Fiber for Use as Fiber Laser, Selected Topics on Optical Fiber Technology, Dr Moh. Yasin (Ed.), ISBN: 978-953-51-0091-1, InTech, Available from: <http://www.intechopen.com/books/selected-topics-on-optical-fiber-technology/fabrication-of-large-core-yb2o3-doped-phase-separated-yttria-alumino-silicate-nano-particles-based-o>

**INTECH**  
open science | open minds

### **InTech Europe**

University Campus STeP Ri  
Slavka Krautzeka 83/A  
51000 Rijeka, Croatia  
Phone: +385 (51) 770 447  
Fax: +385 (51) 686 166  
[www.intechopen.com](http://www.intechopen.com)

### **InTech China**

Unit 405, Office Block, Hotel Equatorial Shanghai  
No.65, Yan An Road (West), Shanghai, 200040, China  
中国上海市延安西路65号上海国际贵都大饭店办公楼405单元  
Phone: +86-21-62489820  
Fax: +86-21-62489821

© 2012 The Author(s). Licensee IntechOpen. This is an open access article distributed under the terms of the [Creative Commons Attribution 3.0 License](#), which permits unrestricted use, distribution, and reproduction in any medium, provided the original work is properly cited.

IntechOpen

IntechOpen